

A multilevel optimization approach to route design and flight allocation taking aircraft sequence and separation constraints into account

Ho-Huu, V.; Hartjes, S.; Pérez-Castán, J. A.; Visser, H. G.; Curran, R.

DOI

[10.1016/j.trc.2020.102684](https://doi.org/10.1016/j.trc.2020.102684)

Publication date

2020

Document Version

Accepted author manuscript

Published in

Transportation Research Part C: Emerging Technologies

Citation (APA)

Ho-Huu, V., Hartjes, S., Pérez-Castán, J. A., Visser, H. G., & Curran, R. (2020). A multilevel optimization approach to route design and flight allocation taking aircraft sequence and separation constraints into account. *Transportation Research Part C: Emerging Technologies*, 117, Article 102684. <https://doi.org/10.1016/j.trc.2020.102684>

Important note

To cite this publication, please use the final published version (if applicable). Please check the document version above.

Copyright

Other than for strictly personal use, it is not permitted to download, forward or distribute the text or part of it, without the consent of the author(s) and/or copyright holder(s), unless the work is under an open content license such as Creative Commons.

Takedown policy

Please contact us and provide details if you believe this document breaches copyrights. We will remove access to the work immediately and investigate your claim.

Transportation Research Part C

A multilevel optimization approach to route design and flight allocation taking aircraft sequence and separation constraints into account

--Manuscript Draft--

Manuscript Number:	TRC_2019_1187R3
Article Type:	Research Paper
Keywords:	airport noise; Trajectory Optimization; conflict detection.; aircraft noise; aircraft separation; aircraft allocation
Corresponding Author:	Vinh Ho-Huu Ton Duc Thang University Ho Chi Minh City, Delft Viet Nam
First Author:	Vinh Ho-Huu
Order of Authors:	Vinh Ho-Huu Sander Hartjes Javier A. Perez-Castan Hendrikus Visser Richard Curran
Abstract:	<p>This paper presents the development of a multilevel optimization framework for the design and selection of departure routes, and the distribution of aircraft movements among these routes, while taking the sequence and separation requirements for aircraft on runways and along selected routes into account. The main aim of the framework is to minimize aircraft noise impact on communities around an airport, and fuel consumption. The proposed framework features two consecutive steps. In the first step, for each given Standard Instrument Departure (SID), multi-objective trajectory optimization is utilized to generate a comprehensive set of possible alternative routes. The obtained set is subsequently used as input for the optimization problem in the second step. In this step, the selection of routes for each SID and the distribution of aircraft movements among these routes are optimized simultaneously. To ensure the feasibility of optimized solutions for an entire operational day, the sequence and separation requirements for aircraft on runways and along selected routes are included in this second phase. In order to address these issues, three novel techniques are developed and added to a previously developed multilevel optimization framework, viz., a runway assignment model, a conflict detection algorithm, and a rerouting technique. The proposed framework is applied to a realistic case study at Amsterdam Airport Schiphol in the Netherlands, in which 599 departure flights and 13 different SIDs are considered. The optimization results show that the proposed model can offer conflict-free solutions, one of which can lead to a reduction in the number of people annoyed of up to 21%, and a reduction in fuel consumption of 8% relative to the reference case solution.</p>
Suggested Reviewers:	Dan Zachary d.s.zachary@jhu.edu Konstantinos VOGIATZIS kvogiatz@civ.uth.gr Xavier Prats xavier.prats@upc.edu Antonio Filippone A.Filippone@manchester.ac.uk
Response to Reviewers:	

A multilevel optimization approach to route design and flight allocation taking aircraft sequence and separation constraints into account

V. Ho-Huu^{a,b*}, S. Hartjes^c, J. A. Pérez-Castán^d, H. G. Visser^c, R. Curran^c

^a *Division of Computational Mathematics and Engineering, Institute for Computational Science, Ton Duc Thang University, Ho Chi Minh City, Vietnam*

^b *Faculty of Civil Engineering, Ton Duc Thang University, Ho Chi Minh City, Vietnam*

^c *Faculty of Aerospace Engineering, Delft University of Technology, P.O. Box 5058, 2600 GB, Delft, The Netherlands*

^d *Universidad Politécnica de Madrid, ETSIAE, Madrid, 28040, Spain*

E-mails: hohuuvinh@tdtu.edu.vn (V. Ho-Huu)

s.hartjes@tudelft.nl (S. Hartjes)

javier.perez.castan@upm.es (J. A. Pérez-Castán)

h.g.visser@tudelft.nl (H. G. Visser)

r.curran@tudelft.nl (R. Curran)

*Corresponding author: V. Ho-Huu, hohuuvinh@tdtu.edu.vn

Abstract

This paper presents the development of a multilevel optimization framework for the design and selection of departure routes, and the distribution of aircraft movements among these routes, while taking the sequence and separation requirements for aircraft on runways and along selected routes into account. The main aim of the framework is to minimize aircraft noise impact on communities around an airport, and the associated fuel consumption. The proposed framework features two consecutive steps. In the first step, for each given Standard Instrument Departure (SID), multi-objective trajectory optimization is utilized to generate a comprehensive set of possible alternative routes. The obtained set is subsequently used as input for the optimization problem in the second step. In this step, the selection of routes for each SID and the distribution of aircraft movements among these routes are optimized simultaneously. To ensure the feasibility of optimized solutions for an entire operational day, the sequence and separation requirements for aircraft on runways and along selected routes are included in this second phase. In order to address these issues, three novel techniques are developed and added to a previously developed multilevel optimization framework, *viz.*, a runway assignment model, a conflict detection algorithm, and a rerouting technique. The proposed framework is applied to a realistic case study at Amsterdam Airport Schiphol in the Netherlands, in which 599 departure flights and 13 different SIDs are considered. The optimization results show that the proposed model can offer conflict-free solutions, one of which can lead to a reduction in the number of people annoyed of up to 21%, and a reduction in fuel consumption of 8% relative to the reference case solution.

Keywords: trajectory optimization; aircraft allocation; aircraft noise; airport noise; aircraft separation; conflict detection.

37 1. Introduction

38 Air transport is predicted to rapidly increase in the coming years due to its social and economic benefits
39 (Boeing, 2016). The increase in air traffic volume may bring certain advantages to the development of
40 society such as job creation, tourism, and industrial globalization. However, it also causes negative
41 impacts on the quality of life of communities surrounding airports, especially as a result of aircraft noise
42 nuisance and pollutant emissions (Asensio et al., 2017). Aircraft noise has been linked to various human
43 health effects such as cardiovascular diseases, sleep disturbance, hearing loss, communication
44 interference, and annoyance (Janssen et al., 2014; Morrell et al., 1997). Noise impact has been well
45 recognized as one of the most significant factors leading to restrictions on the expansion of flight and
46 airport operations (Rodríguez-Díaz et al., 2017).

47 In an effort to support the sustainable development of air transport, the International Civil Aviation
48 Organization (ICAO) has provided the guideline for air traffic management (ICAO, 2016), and various
49 approaches have been studied and proposed over the years (Casalino et al., 2008; Filippone, 2014; Gardi
50 et al., 2015). In order to reduce noise impact caused by aircraft departure/arrival operations, noise
51 abatement trajectory optimization has been applied to generate optimal trajectories, and a significant
52 reduction in both the number of people affected by aircraft noise and fuel consumption has been reported
53 (Zaporozhets and Tokare, 1998; Braakenburg et al., 2011; Hartjes et al., 2014, 2010, 2016; Ho-Huu et
54 al., 2017, 2018; Hogenhuis et al., 2011; Prats et al., 2011, 2010b, 2010a; Song et al., 2014; Torres et al.,
55 2011; Visser and Wijnen, 2003, 2001; Yu et al., 2016; Zhang et al., 2018). Furthermore, the development
56 of allocation models to distribute aircraft movements over specific routes and runways have contributed
57 to a significant reduction of aircraft noise effects (Chatelain and Van Vyve, 2018; Frair, 1984; Ganić et
58 al., 2018; Ho-Huu et al., 2019a; Kuiper et al., 2012; Zachary et al., 2011, 2010). In addition to the
59 research on aircraft noise reduction, research on improving airport capacity and fuel consumption has
60 been widely conducted (D'Ariano et al. 2015; Sama et al. 2017a, 2017b, 2018, 2019).

61 Although a large effort has been made towards finding suitable options to support the continued
62 growth of air transport, there is still a lack of studies that consider different aspects of flight and airport
63 operations concurrently. In particular, research on the design of optimal routes typically considered only

64 one standard route at a time, while its interaction with other routes was not included, as evident from
65 Refs. (Braakenburg et al., 2011; Hartjes et al., 2014, 2010, 2016; Ho-Huu et al., 2017, 2018; Prats et al.,
66 2011, 2010a; Torres et al., 2011; Visser and Wijnen, 2001, 2003; Zhang et al., 2018). Although optimal
67 routes can offer certain benefits, either in terms of noise impact or fuel burn, from an operational
68 perspective, they might be rather difficult to apply when other factors, such as airspace capacity or
69 aircraft separation, are not taken into account. Meanwhile, research on the allocation of aircraft to
70 current-in-use runways and routes can provide more realistic solutions, as reported in Refs. (Chatelain
71 and Van Vyve, 2018; Frair, 1984; Ganić et al., 2018; Kuiper et al., 2012; Zachary et al., 2011, 2010).
72 However, these studies relied on the assumption that the optimal solutions satisfy operational
73 requirements, such as aircraft sequence and separation. Therefore, the true influence of optimal
74 allocation solutions on these issues has not yet adequately studied. Moreover, since these models only
75 considered standard routes instead of optimized routes, the potential noise and fuel reduction benefits
76 were not fully exploited. As a result, there is a need for the development of methodologies that can
77 exploit the advantages of these two types of problems by considering them simultaneously or in a linked
78 manner.

79 In recent work (Ho-Huu et al., 2019b), a two-step optimization framework was developed that can
80 partly deal with the combination of the above two problems. Owing to the advantages inherited from
81 the combination of optimal route design and the distribution of flights among these routes, the two-step
82 framework revealed the potential to considerably reduce the number of people annoyed and fuel
83 consumption. Furthermore, the study indicated that the application of the two-step approach can help to
84 significantly reduce the complexity of the combined problem, while keeping the quality of solutions at
85 almost the same level as in the fully integrated (one-step) approach. Also, the framework proved to be
86 substantially more efficient in terms of the computational cost and flexibility to adapt to changes in the
87 flight schedules. However, since this research mainly focused on the development and validation of an
88 appropriate approach to cope with the complexity of the combined problem, some other operations-
89 related issues were simplified. Specifically, the capacity limits of routes and runways in the framework
90 were implicitly assumed to be satisfied by enforcing a constraint that limits the number of aircraft
91 movements on each route. Moreover, because the sequence and separation requirements for flights were

92 essentially ignored, the results found were just simple distribution solutions that do not contain any
93 information on individual aircraft movements, such as departure times.

94 As a continued development of the previous work, this paper proposes additional techniques and
95 integrates them into the previous model to help overcome the above-mentioned research gaps. Similar
96 to the previous model, the newly proposed framework also features two consecutive steps, in which Step
97 1 addresses the design of optimal routes, whilst Step 2 copes with the selection of routes and the
98 distribution of flights among selected routes. Since the main research gaps of the previous work relate
99 to Step 2, the problem model in Step 1 remains unchanged. In contrast, the optimization model in Step
100 2 has been reformulated as a result of the introduction of new constraints on the throughput capacity of
101 runways and routes. In order to handle these new constraints, three new tool components are proposed.
102 The first one is the development of a runway assignment model that is used to make sure that the safe
103 separation requirements for all aircraft on runways are satisfied. The second additional component
104 concerns a conflict detection algorithm that is included to check the separation requirements between
105 aircraft along selected routes. Finally, a rerouting technique is proposed to resolve any separation
106 violation between aircraft along the selected routes that still might exist after the conflict detection
107 algorithm has been applied.

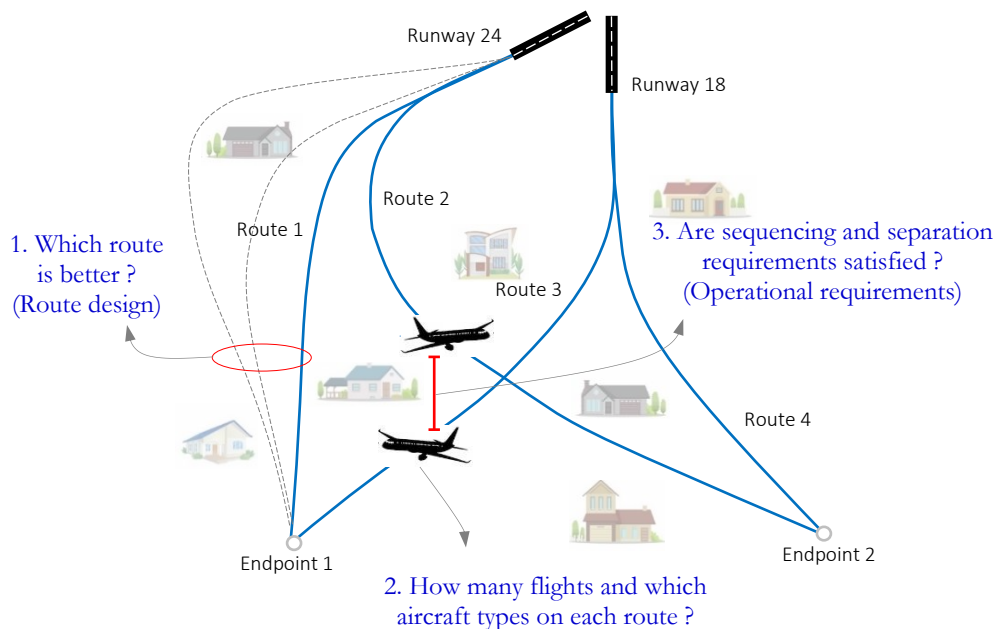
108 The proposed framework is demonstrated through a realistic case study at Amsterdam Airport
109 Schiphol (denoted as AMS), in which a full operational day involving 599 flights and 13 different given
110 standard instrument departure routes are considered. The obtained results are then analyzed and
111 compared with those obtained from the reference case.

112 The remainder of the paper is organized as follows. Section 2 provides a brief introduction of the
113 problem statement. Section 3 presents the proposed framework in detail, including a reformulated two-
114 step optimization approach, a runway assignment model, a conflict detection algorithm, and a rerouting
115 technique. Section 4 provides brief information on the optimization techniques that are used to solve
116 optimization problems in the framework. The application of the proposed framework for a case study at
117 AMS is presented in Section 5. Finally, conclusions are drawn in Section 6.

118

119 **2. Problem statement**

120 Before discussing the functioning of the proposed framework, an example of a representative problem
121 at a generic airport is presented first. Fig. 1 shows a hypothetical example of four Standard Instrument
122 Departure (SID) routes (hereafter referred to as SIDs[†]) and the surrounding communities near an airport.
123 Since noise caused by aircraft operations has significantly negative influences on the quality of life of
124 communities surrounding the airport (in particular, those located near or underneath the routes), the
125 design and selection of routes for each given SID (i.e., Question 1) should be made such as to avoid as
126 many (highly) populated areas as possible. In addition, due to the accumulative nature of noise impact,
127 the distribution of aircraft movements among these routes while guaranteeing aircraft sequence and
128 separation requirements (i.e., Questions 2 and 3) is also an important factor that needs to be considered.
129 Therefore, from a noise perspective, it is apparent that the design and use of noise-optimized routes and
130 the optimal distribution of aircraft movements among these routes emerge as appropriate options that
131 can help to reduce the aircraft noise impact on communities around the airport. However, due to the
132 intricate coupling that exists between these two problems and the associated high computational cost, it
133 is challenging to solve these problems integrally in a single step.



134
135

Fig. 1. An example of routes and communities around an airport.

[†] Please note that the notation of SID is used to denote an existing published Standard Instrument Departure route that connects a given runway to a defined terminal endpoint, while “routes” are used in the context of this paper to represent the optimized ground tracks that are created for each SID by using an optimization algorithm.

136 In this work, a multilevel optimization framework is developed to overcome the complexity of the
 137 integrated problem, as well as the limitations of the computational burden. The main aim of the
 138 framework is to provide solutions that address all three questions together while minimizing the number
 139 of people affected by aircraft noise. Particularly, the final goal of the framework is to determine, for
 140 each given SID, which route is optimal, and how many movements of each aircraft type should be
 141 assigned to this route while taking aircraft sequence and separation requirements into account.
 142 Nevertheless, purely focusing on noise impact may lead to an increase in fuel burn as a result of aircraft
 143 seeking to circumnavigate populated areas. Therefore, fuel consumption is included as a second
 144 objective function in the formulation of the optimization problem. The two objectives are briefly
 145 described below.

146 To determine the Number of People Annoyed (hereafter defined as NPA), the L_{den} -based annoyance
 147 criterion, proposed by EEA (2010), is applied in this study. According to EEA (2010), the percentage
 148 of People Annoyed (%PA) at a given location on the ground is defined as

$$\%PA = 8.588 \times 10^{-6} (L_{den} - 37)^3 + 1.777 \times 10^{-2} (L_{den} - 37)^2 + 1.221 (L_{den} - 37) \quad (1)$$

149 where L_{den} is the day-evening-night noise level, determined by

$$L_{den} = 10 \log_{10} \left[\sum_{k \in N_r} \sum_{i \in N_{at}} \sum_{j \in O_t} a_{ikj} 10^{\frac{SEL_{ik} + w_{den,j}}{10}} \right] - 10 \log_{10} T \text{ (dBA)}, \quad (2)$$

150 where N_r is the total number of given SIDs; N_{at} is the total number of aircraft types; O_t is the operational
 151 time, which includes day, evening and night time; SEL_{ik} is the sound exposure level caused by aircraft
 152 type i on route k ; $w_{den,j}$ is a penalty weighting factor, which is either of 0, 5, or 10 dBA, accounting for
 153 day, evening and night time operations, respectively; a_{ikj} is the number of aircraft type i operating on
 154 route k at the time period j ; and T is the considered period of time in seconds ($T = 24 \times 3600$ seconds in
 155 this case). In Eq. (2), the SEL metric is computed at each location on the ground by using a replication
 156 of the noise model laid down in the technical manual of ECAC (2016).

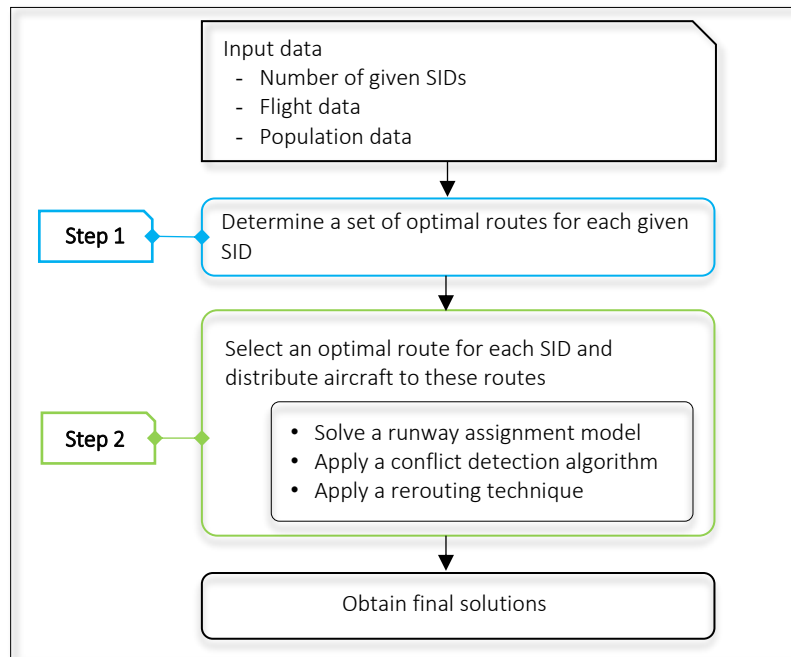
157 The fuel objective is determined as

$$T_{fuel} = \sum_{k \in N_r} \sum_{i \in N_{at}} a_{ik} fuel_{ik} \quad (3)$$

158 where $fuel_{ik}$ is the fuel that aircraft type i consumes when operating on route k . The $fuel_{ik}$ is calculated
 159 by using an intermediate point-mass model (Hartjes et al., 2016) and the Base of Aircraft Data (BADA)
 160 (EUROCONTROL, 2014b).

161 3. A multilevel optimization framework

162 In this section, the proposed multilevel optimization framework is presented in detail. The flowchart of
 163 the framework is illustrated in Fig. 2, while a description of the details will be given in the following
 164 subsections.



165
166

Fig. 2. Flowchart of the multilevel optimization framework.

167 3.1. A two-step approach

168 3.1.1. Step 1: design of optimal routes

169 In order to generate, for each given SID, a set of optimal routes that effectively balances between NPA
 170 and fuel burn, a multi-objective trajectory optimization problem is formulated and solved. The
 171 optimization problem is defined as

$$\min_{\mathbf{p}} \quad (N_{pa}(\mathbf{p}), T_{fuel}(\mathbf{p})) \quad (4)$$

$$\text{s.t.} \quad \mu_i(t) \leq \mu_{\max}(h), \quad \forall i \in N_{at} \quad (5)$$

172 where $N_{pa}(\mathbf{p})$ is the total NPA, and $T_{fuel}(\mathbf{p})$ is the total fuel consumption of all aircraft following the SID.
 173 The design variables are the parameters that define a route; these parameters are collected in the vector
 174 \mathbf{p} . For more details about the definition of the vector \mathbf{p} , interested readers can refer to [Ho-Huu et al.](#)
 175 [\(2017; 2019b\)](#). The variable $\mu_i(t)$ in [Eq.\(5\)](#) is the bank angle of aircraft type i during a turn at time t , and
 176 μ_{max} is the maximum permissible value of μ , varying according to altitude h ([ICAO, 2006](#)).

177 In [Eq. \(4\)](#), the objective $N_{pa}(\mathbf{p})$ is calculated by considering the multiplication of %PA in [Eq. \(1\)](#) in
 178 each grid cell with the population in that cell and subsequent aggregation over all cells. The population
 179 density data surrounding an airport is retrieved from a Geographic Information System (GIS). The
 180 objective $T_{fuel}(\mathbf{p})$ in [Eq. \(4\)](#) is defined similarly as in [Eq. \(3\)](#). It is noted that N_r is now by default equal
 181 to 1 since only one SID at a time is evaluated.

182 The optimization problem is applied for all considered SIDs. The obtained sets of optimal routes
 183 and their associated performances for all SIDs are then utilized as inputs for the optimization problem
 184 in Step 2. It should be noted that to be able to adapt to different runway configurations, the optimal
 185 routes for all given SIDs originating from each runway should be obtained.

186 3.1.2. Step 2: selection of routes and distribution of flight among these routes

187 Before going to the formulation of an optimization problem, it is assumed that the terminal point for
 188 each flight listed in the flight schedule is assumed to be specified in advance, based on its destination
 189 airport. From the sets of optimal routes obtained in Step 1, this step aims to determine, for each given
 190 SID, which route from the set should be selected, as well as to determine how many movements of each
 191 aircraft type should be assigned to this route for an entire day. The formulation of the flight distribution
 192 optimization problem is mathematically formulated as follows.

$$\min_{\mathbf{a}, \mathbf{r}} \quad (N_{pa}(\mathbf{a}, \mathbf{r}), T_{fuel}(\mathbf{a}, \mathbf{r})) \quad (6)$$

$$\text{s.t.} \quad \sum_{k \in SD_s} a_{ik} = T_{a, is}, \quad \forall i \in N_{at}, \forall s \in T_p \quad (7)$$

$$f_d(\mathbf{a}, \mathbf{r}) = 0 \quad (8)$$

$$f_{sr}(\mathbf{a}, \mathbf{r}) \leq 0 \quad (9)$$

$$0 \leq a_{ik} \leq \bar{a}_{ik}, \quad \forall k \in SD_s, \forall i \in N_{at} \quad (10)$$

193 where \mathbf{a} is the design variable vector of flight distribution, in which a_{ik} is the number of aircraft type i
 194 on route k . The vector $\mathbf{r} = \{r_1, \dots, r_k, \dots, r_{Nr}\}$ is the design variable vector of route selection, where the
 195 preferred route r_k is chosen from the set of optimal routes \mathbf{O}_k obtained in Step 1 for SID k . The index s
 196 relates to the terminal point (defined as the endpoint of each departure procedure), and T_p is the set of
 197 terminal points, $s \in T_p$. The vector SD_s is the vector that collects the SIDs which share the same terminal
 198 point s . The parameter $T_{a,is}$ is the total number of aircraft type i assigned to SIDs having the same terminal
 199 point s . Eq. (10) represents the set of boundary constraints on the design variables, where the parameter
 200 \bar{a}_{ik} is the upper bound of the number of aircraft type i on route k , and it can be extracted from the flight
 201 schedule as the total number of aircraft type i assigned to SIDs having the same terminal point. The
 202 function $f_d(\mathbf{a}, \mathbf{r})$ is a constraint imposing the separation requirements between aircraft on the runways
 203 and is defined in the runway assignment model presented in Section 3.2. Similarly, the function $f_{sr}(\mathbf{a}, \mathbf{r})$
 204 is related to safeguarding the separation requirements between aircraft along the selected routes and is
 205 defined in the conflict detection algorithm presented in Section 3.3.

206 In the above optimization problem (Eqs. (6-10)), the objectives $N_{pa}(\mathbf{a}, \mathbf{r})$ and $T_{fuel}(\mathbf{a}, \mathbf{r})$ are defined in
 207 a similar fashion as in Step 1. However, the design variables considered here are different. Particularly,
 208 the design variables in this step represent the routes selected from the sets of available optimal routes
 209 for each SID, and the distribution of flight among these routes. Meanwhile, the design variables in Step
 210 1 are the geometric parameters that are used to construct a SID route. Note that the two objective
 211 functions in Eq. (6) are only calculated if the constraint in Eq. (8) is satisfied; otherwise, large numbers
 212 are assigned to the criteria, representing penalties on an infeasible solution. This avoids the
 213 computationally expensive calculation of the objective values when infeasible solutions are considered.
 214 Also, all the information associated with routes and aircraft types is known a priori in Step 2, as this
 215 information has been stored in Step 1.

216 3.2. Runway assignment model

217 The main objective of the model is to find, for any given instance of (\mathbf{a}, \mathbf{r}) considered in Step 2, a suitable
 218 conflict-free solution for the assignment of individual flights to specific routes and runways, while

219 minimizing the total departure delay (relative to the departure times listed in the flight schedule) at
 220 runways. It is noted that the original objectives in Eq. (6) – NPA and fuel – are the focus of the main
 221 distribution algorithm, which determines which share of the total movements (for each aircraft type) are
 222 assigned to a specific route. In other words, the flight distribution optimization problem only considers
 223 the flows of aircraft movements. The flight to runway assignment model, on the other hand, merely
 224 determines how individual flights are assigned to runways, essentially looking for a conflict-free
 225 realization at the runways of the flow solution generated by the flight distribution optimization
 226 algorithm, taking departure times into account. Therefore, the flight to runway assignment has no impact
 227 on the original objectives NPA and fuel. It is important to note that although the runway assignment
 228 model yields solutions that are free of conflict at the departure runway, separation conflicts might still
 229 occur down-route. The handling of potential down-route conflicts is discussed in Section 3.3. It is also
 230 important to note that when a flight is assigned to a runway, its route is automatically determined. The
 231 flight to runway assignment model is mathematically written as follows.

$$\min_{\mathbf{x}, \mathbf{d}} \quad \sum_{j \in J} d_j \quad (11)$$

$$\text{s.t.} \quad (t_{j+1} + d_{j+1}) - (t_j + d_j) - Mx_{j+1}^r - Mx_j^r \geq t_s - 2M, \forall j \in J, \forall r \in R \quad (12)$$

$$(t_{j+1} + d_{j+1}) \geq (t_j + d_j), \forall j \in J \quad (13)$$

$$\sum_{r \in R} x_j^r = 1, \forall j \in J \quad (14)$$

$$\sum_{j \in J} c_{jis} x_j^r = N_{is}^r, \forall i \in N_{at}, \forall s \in T_p, \forall r \in R \quad (15)$$

232 where \mathbf{x} is the vector of binary design variables x_j^r , in which x_j^r represents the assignment of flight j to
 233 runway r , $x_j^r \in \{0,1\}$. The vector \mathbf{d} is the vector of delay variables d_j , where d_j ($d_j \geq 0$) represents the
 234 departure delay of flight j at the runway. The parameters J and R are, respectively, the set of flights in
 235 the flight schedule and the set of runways. The parameter t_j is the scheduled departure time of flight j ,
 236 and t_s is the required time separation, which depends on the weight classes of following and leading
 237 aircraft, as indicated in EUROCONTROL (2018) (see Table 1). Note that the empty fields in Table 1
 238 indicate a minimum departure interval of 60 seconds (Delsen, 2016). The parameter c_{jis} is the constraint
 239 coefficient of flight j that is associated with aircraft type i and terminal point s . The coefficient c_{jis} will

240 be equal to 1 if flight j of aircraft type i flies to terminal point s , otherwise it will be equal to 0. The
 241 parameter N_{is}^r is the total number of aircraft type i departing from runway r to terminal point s . It is
 242 noted that, for any instance of (\mathbf{a}, \mathbf{r}) produced by the aircraft distribution optimization algorithm, the
 243 parameters N_{is}^r can be determined up front from the flight schedule information.

244 **Table 1.** RECAT-EU wake turbulence time-based separation minima on departure (EUROCONTROL,
 245 2018).

RECAT-EU scheme		"SUPER HEAVY"	"UPPER HEAVY"	"LOWER HEAVY"	"UPPER MEDIUM"	"LOWER MEDIUM"	"LIGHT"
Leader / Follower		"A"	"B"	"C"	"D"	"E"	"F"
"SUPER HEAVY"	"A"		100s	120s	140s	160s	180s
"UPPER HEAVY"	"B"				100s	120s	140s
"LOWER HEAVY"	"C"				80s	100s	120s
"UPPER MEDIUM"	"D"						120s
"LOWER MEDIUM"	"E"						100s
"LIGHT"	"F"						80s

246

247 In the optimization problem (Eqs. (11-15)), the objective function represents the minimization of
 248 the total departure delay. The first constraint aims to ensure that the separation requirement between two
 249 consecutive aircraft on the same runway is always satisfied. The parameter M in the constraint is a large
 250 number (e.g., 10^6) that helps to render the constraint inactive in the case that two consecutive aircraft
 251 are assigned to two different runways. For example, if two consecutive aircraft are assigned to two
 252 different runways (i.e., $x_j^r = 1$ and $x_{j+1}^r = 0$ or $x_j^r = 0$ and $x_{j+1}^r = 1$), and the separation time between
 253 them is smaller than t_s , the constraint is still satisfied, which can be readily inferred from Eq. (12). In
 254 contrast, if two consecutive aircraft are assigned to the same runway, the separation between them has
 255 to be larger than t_s ; otherwise, the allocation solution is infeasible. The second constraint Eq. (13) ensures
 256 that the sequence of flights listed in the flight schedule is kept unchanged when departure delays are
 257 introduced. The third constraint guarantees that each flight is assigned to one runway only. Finally, the
 258 last constraint aims to ensure that the assignment of aircraft on each runway always matches the

259 information of the distribution variables in the main optimization problem in Step 2 and complies with
260 the flight information and aircraft sequence as given in the flight schedule.

261 In order to determine the constraint Eq. (8) in Step 2, the function $f_d(\mathbf{a}, \mathbf{r})$ is defined as

$$f_d(\mathbf{a}, \mathbf{r}) = \sum_{j \in J} d_j - \bar{D} \quad (16)$$

262 where \bar{D} is the total delay at the runways, which is derived from the runway assignment problem
263 without considering the distribution constraint Eq. (15). Therefore, the delay \bar{D} is independent from the
264 solution (\mathbf{r}, \mathbf{a}) and can be calculated up front by solving the optimization problem in Eqs. (11-14) based
265 on a given flight schedule and set of available runways. Meanwhile, the delay $\sum d_j$ in Eq. (16) associated
266 to a solution instance (\mathbf{r}, \mathbf{a}) might be influenced by the inclusion of the constraint Eq. (15). Since the
267 problem in Eqs. (11-14) represents a relaxation of the problem in Eqs. (11-15), the value of \bar{D} will not
268 exceed that of $\sum d_j$. Therefore, the constraint $f_d(\mathbf{a}, \mathbf{r}) = 0$ enforced in Eq.(8) makes sure that the solutions
269 obtained by the optimization problem in Step 2 do not cause a delay compared with the delay \bar{D} , and
270 hence the runway capacity is kept at the maximum level.

271 3.3. Conflict detection algorithm

272 Once the result of the runway assignment model has been returned, an additional check is carried out
273 with respect to the satisfaction of constraint Eq. (9) along the routes. If the returned result does not
274 satisfy the delay constraint Eq. (8), the check is no longer needed, and a large penalty number is assigned
275 to this constraint. Otherwise, a conflict detection algorithm will be evoked to check the separation
276 requirement of aircraft along the selected routes.

277 From the flight schedule and the assignment solution returned by the assignment model, the route
278 information and associated performance can be obtained for each flight. This information comprises the
279 flight trajectory (i.e., position coordinates, velocity, altitude, time), fuel burn and noise value (i.e., SEL).
280 After the trajectories for all flights in the flight schedule have been defined, a simulation process is
281 carried out for all flights contained in the schedule, using an iteration time step of 10 seconds (as
282 suggested by Isaacson and Erzberger (1997)). In order to check the aircraft separation requirements in
283 both vertical and horizontal dimensions, the distance separation minima suggested by ICAO (2016) and

284 EUROCONTROL (2018) is applied. The vertical separation is set to 1,000 ft (ICAO, 2016), while the
 285 horizontal separation standards are given in Table 2 (EUROCONTROL, 2018). The horizontal
 286 separation is defined here as the Euclidean distance in the horizontal plane between the aircraft in each
 287 pair (Isaacson and Erzberger, 1997; Visser, 2008). It is noted that the separation minima indicated in
 288 Table 2 are applied to flights operating on the same routes, while for those operating on different routes,
 289 a minimum radar separation of 3 NM is enforced. It should also be noted that only the wake vortex
 290 separation minima are enforced and that all runways are assumed to be operated independently, i.e.,
 291 departures can take place simultaneously at all runways. The main procedure of the algorithm is
 292 described in Algorithm 1.

293 Table 2. RECAT-EU wake turbulence distance-based separation minima on approach and departure.
 294 (EUROCONTROL, 2018).

RECAT-EU scheme		"SUPER HEAVY"	"UPPER HEAVY"	"LOWER HEAVY"	"UPPER MEDIUM"	"LOWER MEDIUM"	"LIGHT"
Leader / Follower		"A"	"B"	"C"	"D"	"E"	"F"
"SUPER HEAVY"	"A"	3 NM	4 NM	5 NM	5 NM	6 NM	8 NM
"UPPER HEAVY"	"B"		3 NM	4 NM	4 NM	5 NM	7 NM
"LOWER HEAVY"	"C"		(*)	3 NM	3 NM	4 NM	6 NM
"UPPER MEDIUM"	"D"						5 NM
"LOWER MEDIUM"	"E"						4 NM
"LIGHT"	"F"						3 NM

(*) means minimum radar separation (MRS), set at 2.5 nautical mile (NM), is applicable as per current ICAO doc 4444 provisions.

295
 296
 297
 298

```

Input:
- Flight data;
- Route trajectories;
- Time step; starting time, ending time;
- Set the couple of flights violating the required distance separation ( $VS$ ) to 0,  $VS = 0$ ;
For each time step
    Define flights entering into the time window;
    Extract the flight trajectories for these flights;
    Calculate the vertical distance for each couple of flights;
    For each couple of flight
        If the vertical separation is violated
            Calculate the horizontal distance
            If the horizontal separation is violated
                Set  $VS = VS + 1$ ;
            End
        End
    End
End

```

Output: A set of couple of flights violating the required separation, VS .

300 Once the algorithm has terminated, the number of instances of flights violating the required distance
301 separation standards is stored in the parameter VS . If VS is equal to 0, the constraint in Eq. (9) is satisfied,
302 and hence the allocation solution is feasible. Otherwise, the allocation solution is infeasible.

303 It should be noted that the resolution of the runway assignment problem in Section 3.2 may lead to
304 a situation in which multiple (non-unique) optimal solutions are found. Since the assignments of aircraft
305 on runways for the various optimal solutions may lead to different conflict situations down-route, the
306 conflict algorithm will be applied for each optimal solution obtained by the runway assignment model.
307 Subsequently, the solution without any conflicts or that with the smallest number of conflict cases is
308 selected. In the latter case, the rerouting technique will be subsequently applied to the identified
309 conflicting flights and will be presented in detail in the following section.

310 3.4. Rerouting technique

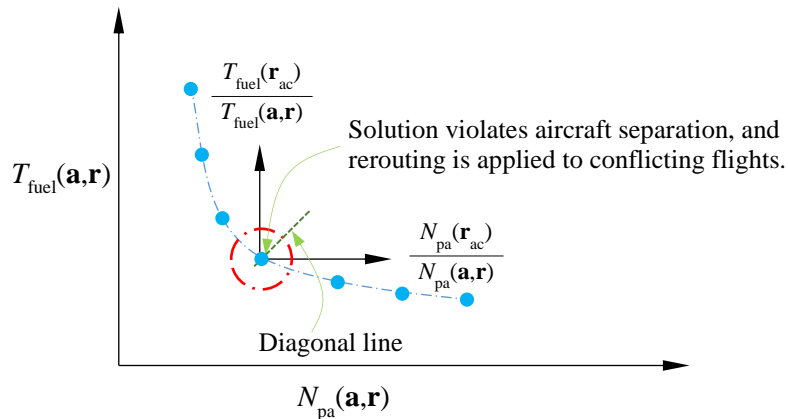
311 The conflict detection algorithm is applied to every distribution solution obtained for the optimization
312 problem in Eqs. (6-10). If any couple of flights in these solutions violate separation minima which is
313 discovered by the conflict detection algorithm, a rerouting technique is used. The idea behind the
314 rerouting method is similar to that of the vectoring solutions as currently issued by Air Traffic
315 Controllers (ATC), which is used to resolve the conflict between flights listed in the schedule when they
316 fly along the selected routes. In the rerouting method, alternative routes are assigned to each pair of

317 flights whose separation distances violate the specified minima while still optimizing noise impact and
 318 fuel consumption. To this end, an optimization problem is formulated and solved for each pair of
 319 conflicting flights in the flight distribution solution. The associated optimization problem is written as
 320 follows.

$$\min_{\mathbf{r}_{ac}} w_1 \frac{N_{pa}(\mathbf{r}_{ac})}{N_{pa}(\mathbf{a}, \mathbf{r})} + w_2 \frac{T_{fuel}(\mathbf{r}_{ac})}{T_{fuel}(\mathbf{a}, \mathbf{r})} \quad (17)$$

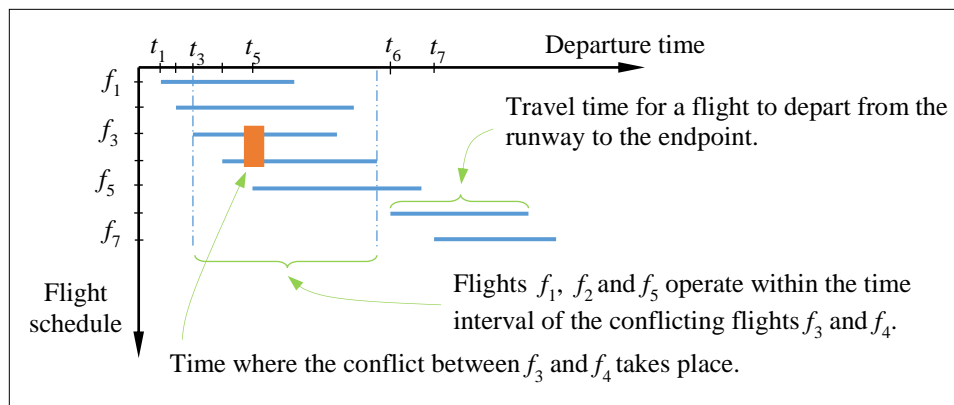
$$\text{s.t. } f_{sr}(\mathbf{r}) = 0 \quad (18)$$

321 where \mathbf{r}_{ac} is the design variable vector of alternative routes for the pair of conflicting flights whose
 322 separation violates the separation standard; the alternative routes are again selected from the sets of
 323 optimal routes obtained in Step 1. The objective function is the normalization of the NPA and fuel
 324 consumption, in which $N_{pa}(\mathbf{r}_{ac})$ and $T_{fuel}(\mathbf{r}_{ac})$ are the NPA and the total fuel burn associated with new
 325 alternative routes for conflicting flights, respectively; and $N_{pa}(\mathbf{a}, \mathbf{r})$ and $T_{fuel}(\mathbf{a}, \mathbf{r})$ are, respectively, the
 326 NPA and the total fuel burn associated with the design variables of the optimization problem in Eqs. (6-
 327 10). Note that $N_{pa}(\mathbf{a}, \mathbf{r})$ and $T_{fuel}(\mathbf{a}, \mathbf{r})$ are known at this stage. The parameters w_1 and w_2 are the weighting
 328 factors, which are used to transfer a bi-objective optimization problem into a single objective one. In
 329 this case, w_1 and w_2 are set to 0.5 with the aim of giving an equal priority to both the NPA and fuel
 330 consumption. This setting also aims to retain the diversity of solutions in the original Pareto front. As
 331 illustrated in Fig. 3, due to the use of the equivalent weight of 0.5 for both objectives, the solution
 332 obtained by the optimization problem in this section is expected to be located along the dotted diagonal
 333 line, which is the line having an angle of 45 degrees relative to the horizontal axis.



334 Fig. 3. Illustration of the optimal solution of the optimization problem in Eqs. (17-18).
 335
 336

337 The evaluation of the constraint is performed by evoking the conflict detection algorithm in [Section](#)
338 [3.3](#). In this case, however, only flights involved in a time interval, within which conflict between flights
339 take place, are taken into account. The time interval is determined by the total travel time of the pair of
340 conflicting flights from the runways to the endpoints. To make sure the selection of new routes for the
341 conflicting flights do not cause any conflicts to other flights outside of the time interval, the travel time
342 of the conflicting flights is estimated based on the longest route stored in the set of available routes for
343 each SID. The determination of the time interval and the identification of flights within this interval is
344 illustrated in [Fig. 4](#). In the figure, the two conflicting flights are f_3 and f_4 ; the time interval is delimited
345 by the starting time of flight f_3 and the ending time of flight f_4 ; and the flights involved in this time
346 interval are f_1, f_2 , and f_5 . Since only flights operating within the time interval are considered, the rerouting
347 of conflicting flights does not influence flights outside this time interval. Furthermore, since typically
348 only a few flights in the flight schedule are involved, the computational cost of solving the problem in
349 this step is relatively small, just a few seconds of CPU time.



350
351 **Fig. 4.** Illustration of the number of flights involved in the time interval within which the conflict takes
352 place.

353 When the conflict detection tool identifies more than one pair of conflicting aircraft, the rerouting
354 algorithm is sequentially applied to each conflicting pair. Note that the rerouting technique is applied to
355 every distribution solution obtained for the optimization problem in [Eqs. \(6-10\)](#) if the solution contains
356 any couple of flights violating the separation standard.

357

358

359 4. Optimization techniques

360 As can be seen in Section 3, four different optimization problems have been established. The first two
361 problems are nonlinear multi-objective parameter optimization problems. The third problem is a mixed
362 integer linear programming problem (MILP) which is nested in the second problem, and the last one is
363 a nonlinear single-objective parameter optimization problem. To solve these four problems, four
364 different optimization methods are used. For the first problem (Eqs. (4-5)), the Multi-objective
365 Optimization Evolutionary Algorithm based on Decomposition (MOEA/D), as proposed by Zhang and
366 Li (2007) and improved by Ho-Huu et al. (2017), is applied. This choice is motivated by the fact that
367 MOEA/D has been demonstrated to be an efficient method to deal with this type of problems (Ho-Huu
368 et al., 2017). Meanwhile, the Non-dominated Sorting Genetic Algorithm (NSGA-II) (Deb et al., 2002)
369 is utilized to solve the second problem (Eqs. (6-10)). The preference for this method is, in this case,
370 because the design space of this problem is very restricted, and hence the solutions easily violate the
371 constraints. Therefore, NSGA-II is more suitable than MOEA/D in this case. A mixed integer linear
372 solver from the CPLEX optimization suite/library is applied to solve the linear optimization problem
373 (Eqs. (11-15)). Finally, the last problem (Eq. (17-18)) is solved by using the Differential Evolution (DE)
374 algorithm (Storn and Price, 1997). For more details on MOEA/D, NSGA-II, and DE, interested readers
375 are referred to Refs. (Ho-Huu et al., 2017; Zhang and Li, 2007), (Storn and Price, 1997), and (Deb et
376 al., 2002), respectively. It should be noted that, in order to deal with the equality constraint in Eq. (7), a
377 constraint handling technique developed in (Ho-Huu et al., 2018) has been applied and coupled to the
378 NSGA-II algorithm. Please note that since some of the applied optimization methods, including
379 MOEA/D, NSGA-II and DE, are heuristic methods, the solutions obtained by these methods are only
380 approximate or nearly optimal solutions. **As a consequence, the word “optimized” is used in the later
381 section instead of “optimal” to express the obtained solutions when the above-mentioned optimization
382 techniques are applied to solve the optimization problems.**

383

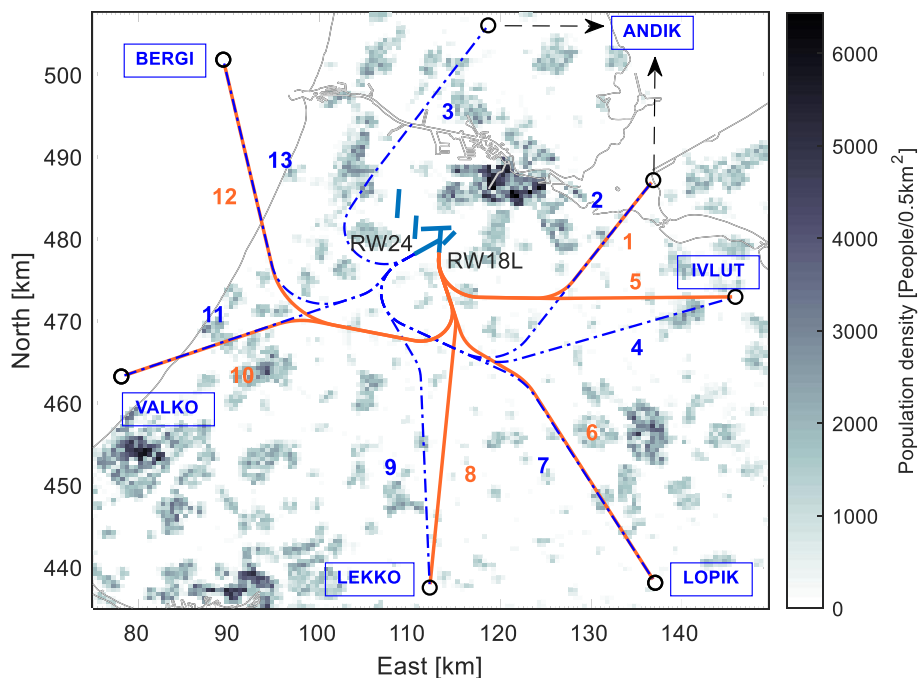
384

385 **5. Numerical results and discussion**

386 In this section, the reliability and efficiency of the proposed framework are evaluated using a realistic
387 case study at Amsterdam Airport Schiphol (denoted as AMS) in The Netherlands. On the selected
388 reference day, 599 departure flights were recorded, that operated on two runways, viz., RWs 24 and 18L
389 (Dons, 2012), as shown in Fig. 5.



390
391 **Fig. 5.** Illustration of real departure operations at AMS.



392
393 **Fig. 6.** Illustration of departure routes at AMS.

394 According to the flight data and the Aeronautical Information Publication (AIP)[‡], 13 distinct SIDs
 395 were in use on the reference day, as shown in Fig. 6. In the figure, the solid routes originating from
 396 RW18L are highlighted and numbered in orange, while the dashed routes originating from RW24 are
 397 highlighted and numbered in blue. There are 6 terminal points (defined as the endpoints of departure
 398 procedures in this study), viz. ANDIK, IVLUT, LOPIK, LEKKO, VALKO and BERGI. Each terminal
 399 point is connected by two routes originating from either RW24 or RW18L, except for ANDIK that is
 400 connected by three routes, consisting of route 1 from RW18L and routes 2 and 3 from RW24. Note that,
 401 from the assignment solution produced by the runway assignment model, the assignment of flights to
 402 routes for the terminal points IVLUT, LOPIK, LEKKO, VALKO, and BERGI is automatically known,
 403 as there is only a single route available from each runway.

404 However, for the terminal point ANDIK, two different routes are available from RW24 runway,
 405 and hence an additional step is needed. To determine which flight is assigned to either route 2 or 3 from
 406 RW24, the following heuristic rule is applied. In order to reduce the number of potential crossing
 407 conflicts between flights during the peak hours, flights operating in this time period are assigned to route
 408 3 until its capacity limit is reached; the remainder of the flights are assigned to route 2.

409 Though many different aircraft types operate on these routes, for the sake of simplicity, all flight
 410 movements are represented here by either of three aircraft types, namely, Fokker 100 (F100), Boeing
 411 737-800 (B738), and Boeing 777-300 (B773). It is assumed that the F100, B738, and B773, respectively,
 412 represent lower medium (LM), upper medium (UM) and upper heavy (UH) aircraft, as classified by
 413 EUROCONTROL (2015). The population data provided by the Dutch Central Bureau of Statistics
 414 (CBS) (Centraal Bureau voor de Statistiek) with a grid cell size of 500 x 500 m, as shown in Fig. 6, is
 415 used. The detailed data of aircraft movements is provided in Table 3. All the simulations are carried out
 416 in MATLAB 2018b on an Intel Core i5 and 8GB RAM desktop.

417 **Table 3.** The detailed data for aircraft operations.

Terminal point	Number of aircraft movements			
	Entire day [LM, UM, UH]	Day (7h00-19h00) [LM, UM, UH]	Evening (19h00-23h00) [LM, UM, UH]	Night (23h00-7h00) [LM, UM, UH]
ANDIK	[45, 22, 8]	[32, 14, 3]	[6, 6, 5]	[7, 2, 0]
IVLUT	[74, 98, 43]	[57, 69, 28]	[9, 10, 12]	[8, 19, 3]
LOPIK	[7, 11, 2]	[4, 9, 2]	[2, 1, 0]	[1, 1, 0]
LEKKO	[35, 76, 3]	[30, 46, 3]	[3, 8, 0]	[2, 22, 0]

[‡] <https://www.lvn.nl/eaip/2019-12-19-AIRAC/html/index-en-GB.html> (accessed 2 January 2020).

VALKO	[36, 31, 12]	[27, 24, 10]	[4, 4, 1]	[5, 3, 1]
BERGI	[34, 26, 36]	[27, 18, 35]	[4, 7, 0]	[3, 1, 1]
Total	[231, 264, 104]	[177, 180, 81]	[28, 36, 18]	[26, 48, 5]

418

419 5.1. Evaluation of the distribution model in Step 2

420 Since the aircraft sequence and separation requirements are considered and integrated into the
421 distribution model in Step 2, it is important to investigate the performance of this model independently.
422 The main aim of this investigation is to see whether, based on the current SIDs, the model can provide
423 better distribution options to reduce noise impact and fuel consumption compared with the reference
424 case.

425 Before executing the model, the reference case is determined first. The reference case considers the
426 599 flights, as shown in Fig. 5. It is noted that due to capacity reasons, the flights in Fig. 5 have been
427 vectored by Air Traffic Controllers (ATC). In order to make the calculation of the reference case simpler,
428 it is assumed here that all vectored flights are simply assigned to one of the fixed routes as shown in Fig.
429 6. By recreating the traffic flow based on the reference data (which include the actual departure times)
430 and the standard routes as defined in Fig. 6, the number of people annoyed and the total fuel burn in ton
431 are 75,800 and 332.20, respectively, and there is no delay at the runways, i.e., $\bar{D}=0$. The result also
432 shows that 8 cases of flights which violate the required separation minima emerge. Nevertheless, the
433 number of conflicting flights remains small, representing less than 2% of the total traffic volume. For
434 comparison purposes, therefore, it is assumed that all distribution solutions derived from the distribution
435 model are deemed acceptable if they feature less than 8 violations.

436 To solve the problem defined by Eqs. (6-10), the NSGA-II algorithm with a population size of 70
437 and a maximum number of 1500 generations (Gen.), as used in Ho-Huu et al. (2019a), is applied. Fig. 7
438 shows the optimized results obtained by the distribution model and the solution to the reference case.
439 As expected, it can be seen from Fig. 7 that all the solutions from the model dominate that of the
440 reference case and are much better in both the NPA and fuel consumption. In addition, only 7 violations
441 are recorded for solutions obtained by the proposed model, which is one case less compared with that
442 of the reference scenario. Note that in this section the rerouting technique is not yet applied.

443 Regarding the performance of the optimization algorithm, it can be seen from Fig. 8 that the
 444 algorithm has a good convergence rate. After 1200 generations, the solutions start to converge, and there
 445 are no significant changes after 1300 generations. The total time for the algorithm to reach the final
 446 generation is 7.39 hours. It should be noted that because the flight schedule can be obtained some days
 447 in advance, the model can be used as a planning tool to deliver reasonable solutions for the assignment
 448 of flights a priori. Furthermore, owing to the independent evaluation of objective functions in the
 449 optimization algorithm, the computational cost of the distribution problem can be further improved by
 450 using parallel computing with multiple cores or cluster computing.

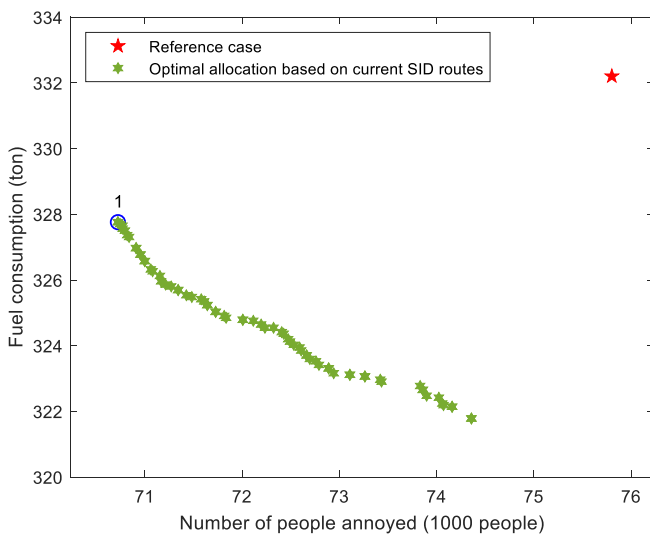


Fig. 7. Comparison of the NPA and fuel consumption obtained for the reference case and the optimized distribution solutions based on the current SID routes.

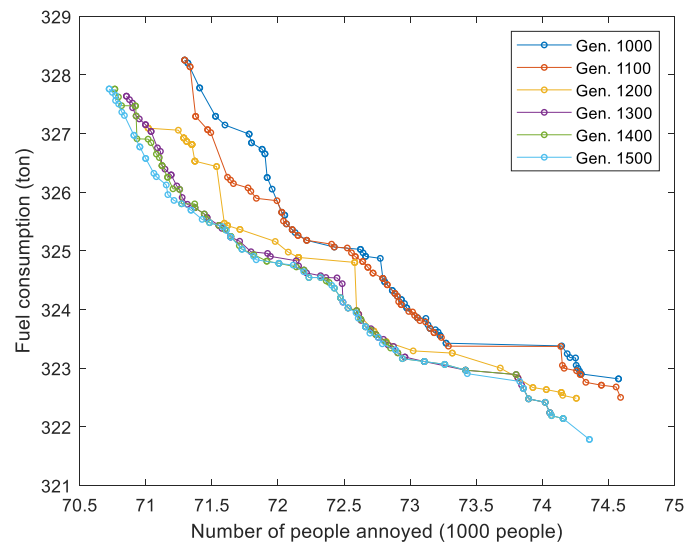
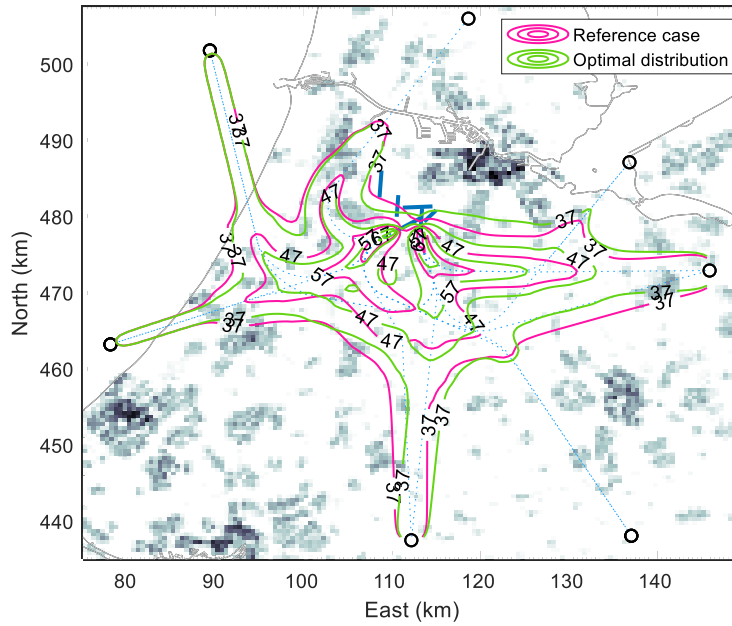


Fig. 8. Convergence history of the optimized distribution solutions based on the current SID routes.

451 To further examine the advantage of the model, a single representative solution, i.e., solution 1 as
 452 highlighted in Fig. 7, is selected for further analyses. The L_{den} noise contours associated to this solution
 453 are illustrated in Fig. 9, along with those resulting from the reference case. As can be seen from the
 454 figure, there is a distinct difference in the size of the L_{den} contours between the two solutions. Indeed,
 455 the contours associated with solution 1 appear to avoid populated regions better than those associated to
 456 the reference case, hence leading to a reduction in the NPA.

457



458
459 **Fig. 9.** Comparison of the L_{den} noise contours caused by the reference case and the optimized distribution
460 solution (solution 1) based on current SIDs.

461 To provide a better understanding of the reason leading to the change of the contours in **Fig. 9**, the
462 distribution of flights among the routes obtained in solution 1 is also provided numerically in **Table 4**.
463 At first glance, it can be noted in **Table 4** that there is a large shift of aircraft movements between routes
464 8 and 9. Specifically, on route 8 in the reference case, there are 44 daytime flights (21 F100s, 20 B738s
465 and 3 B773s), 11 evening flights (3 F100 and 8 B738s), and no night flights, whilst in solution 1 there
466 are 74 daytime flights (27 F100s, 44 B738s and 3 B773s), 10 evening flights (2 F100s and 8 B738s),
467 and up to 24 night flights (2 F100s and 22 B738s). This redistribution of movements explains why in
468 **Fig. 9** the contours shift to the right of routes 8 and 9, which, evidently, results in a reduction in the
469 NPA. Moreover, since the track along route 8 is shorter than that of route 9, more aircraft are assigned
470 to route 8, and more fuel can be saved. The same situation can also be observed in the distribution of
471 flights among routes 4 and 5, contributing to a significant reduction in fuel burn as a result of aircraft
472 flying on a shorter route.

473 **Table 4.** Comparison of flight distribution obtained by the reference case and the optimized distribution solution
474 (solution 1) based on current SIDs.

Route number	Approach	Day			Evening			Night		
		F100	B738	B773	F100	B738	B773	F100	B738	B773
1	RC*	0	0	0	2	2	2	0	0	0
	OD#	11	10	2	2	4	3	7	2	0
2	RC	3	5	2	0	1	1	7	2	0
	OD	0	0	0	0	0	0	0	0	0
3	RC	29	9	1	4	3	2	0	0	0
	OA	21	4	1	4	2	2	0	0	0
4	RC	20	31	15	1	2	1	8	19	3

	OD	3	2	3	0	0	3	0	0	0
	RC	37	38	13	8	8	11	0	0	0
5	OD	54	67	25	9	10	9	8	19	3
	RC	3	6	0	2	1	0	0	0	0
6	OD	3	9	2	2	1	0	1	1	0
	RC	1	3	2	0	0	0	1	1	0
7	OD	1	0	0	0	0	0	0	0	0
	RC	21	20	3	3	8	0	0	0	0
8	OD	27	44	3	2	8	0	2	22	0
	RC	9	26	0	0	0	0	2	22	0
9	OD	3	2	0	1	0	0	0	0	0
	RC	0	0	0	0	2	0	0	0	0
10	OD	13	17	4	0	1	1	5	3	1
	RC	27	24	10	4	2	1	5	3	1
11	OD	14	7	6	4	3	0	0	0	0
	RC	0	0	0	0	3	0	0	0	0
12	OD	2	7	13	1	3	0	1	1	1
	RC	27	18	35	4	4	0	3	1	1
13	OD	25	11	22	3	4	0	2	0	0

475 RC*: Reference Case; OD#: Optimized Distribution

476 Based on the results obtained above, it can be concluded that the distribution model in Step 2 is
477 reliable and effective. The proposed model can provide better distribution options in terms of both noise
478 impact and fuel consumption.

479 5.2. Evaluation of the entire framework

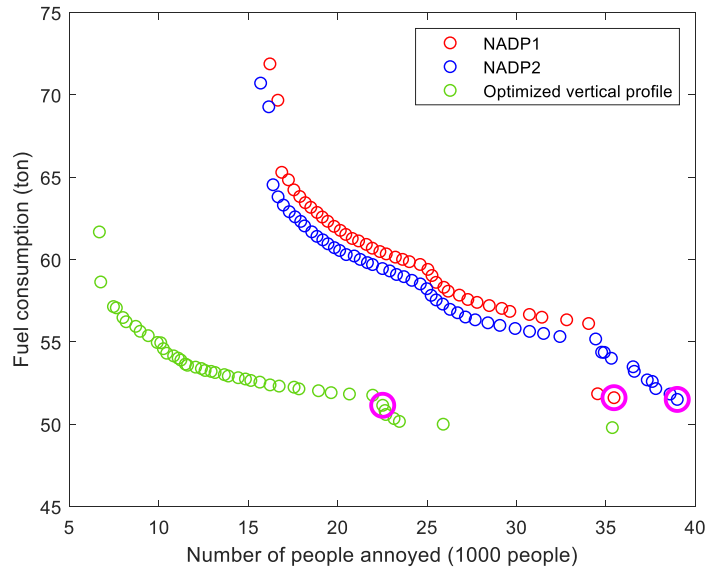
480 In this section, the performance of the framework in its entirety is evaluated. However, in Step 1 of the
481 framework, the set of optimized routes for each given SID can be obtained by using either 2D
482 optimization or 3D optimization. For the 2D optimization, only ground tracks are optimized while
483 vertical profiles comply with standard departure procedures, such as Noise Abatement Departure
484 Procedures 1 and 2 (NADP1, NADP2) (ICAO, 2006). For the 3D optimization, both ground tracks and
485 vertical profiles are optimized simultaneously. Therefore, before generating the optimized solutions, a
486 comparison of these two approaches is first carried out in the next subsection. This comparison also
487 aims to provide a better understanding of the final optimized solutions for the complete problem, which
488 will be considered in [Section 5.2.2](#).

489 5.2.1. A comparison of optimized routes based on the different settings of vertical profiles

490 In order to evaluate the influence of the vertical profiles, including NADP1, NADP2, and optimized
491 vertical profiles, on the noise impact and fuel consumption, three distinct optimization problems
492 corresponding to three different vertical profile scenarios are performed for an example route. For this

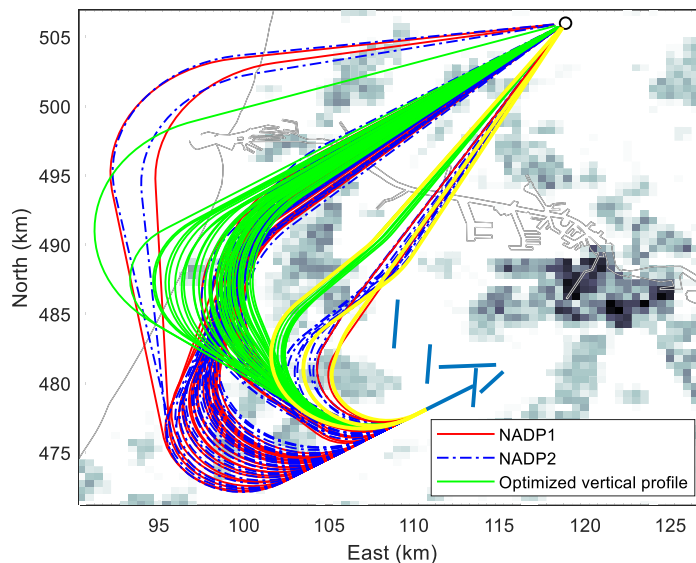
493 comparison, route 3 is used. The evaluation is also a first study that compares the two different settings
494 of vertical profiles in the field of the aircraft route design problem. To determine optimized solutions,
495 the number of aircraft, as indicated in [Table 3](#) for the terminal point ANDIK with an additional 30% of
496 traffic (which accounts for a potential increase in the number of movements due to the application of
497 the distribution algorithm), is applied. For further details on the motivation to add 30% extra traffic,
498 interested readers are encouraged to read [Ho-Huu et al. \(2019b\)](#). For each optimization problem, aircraft
499 of all types follow a shared ground track, but each with its own distinct vertical profile, which is either
500 a standard procedure or an optimized vertical profile. A SID is assumed to start at the end of the runway
501 at an altitude of 35 ft AGL and at a take-off safety speed V_{2+10} kts, and to terminate at an altitude of
502 6,000 ft and an equivalent airspeed of 250 kts. To solve the three optimization problems, the MOEA/D
503 algorithm with a population size of 50 and a maximum of 1,000 generations, as used in [Ho-Huu et al.](#)
504 [\(2017\)](#), is applied. To generate optimized routes for each SID in Step 1 of the framework, the same
505 approach is also applied to all the 13 SIDs.

506 The optimized solutions are shown in [Fig. 10](#). It can be seen in [Fig. 10](#) that, as expected, the
507 optimized vertical profile is the best approach and significantly outperforms NADP1 and NADP2, while
508 NADP2 generally performs better than NADP1. A closer look at [Fig. 10](#) shows that there are still two
509 NADP1-based solutions that dominate some of the NADP2-based solutions. The reason for this is that,
510 due to the focus on climbing in the initial phase of the departure, the airspeed in a NADP1 is lower than
511 for a NADP2. The lower airspeed allows aircraft to make tighter turns over less populated regions while
512 still satisfying the bank angle constraints, as defined by [Eq. \(5\)](#).

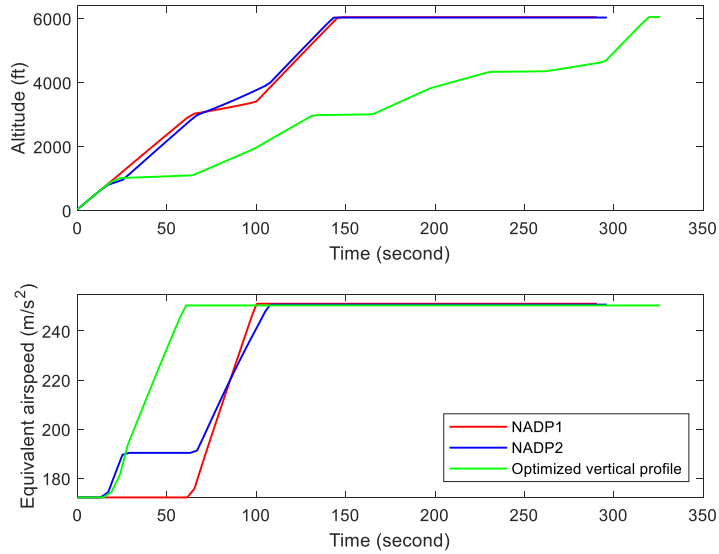


513
514 **Fig. 10.** Comparison of the optimized solutions obtained by NADP1, NADP2 and optimized
515 vertical profiles.

516 **Fig. 11** illustrates the optimized ground tracks obtained for three different optimization problems.
517 It can be observed in **Fig. 11** that all ground tracks attempt to avoid populated areas as far as possible.
518 While the differences between the ground tracks obtained by using NADP1 and NADP2 are small, they
519 are quite significant between those obtained by 3D optimization and 2D optimization. For a better
520 understanding of the combination of ground tracks and vertical profiles, some representative solutions
521 of each case, as highlighted in **Fig. 11** in yellow, are selected. The vertical profiles derived from a B738
522 for each approach are depicted in **Fig. 12**. It is seen in **Fig. 12** that there is a significant difference in the
523 airspeed profile between the approaches.



524
525 **Fig. 11.** Comparison of optimized ground tracks obtained by NADP1, NADP2 and optimized
526 vertical profiles.

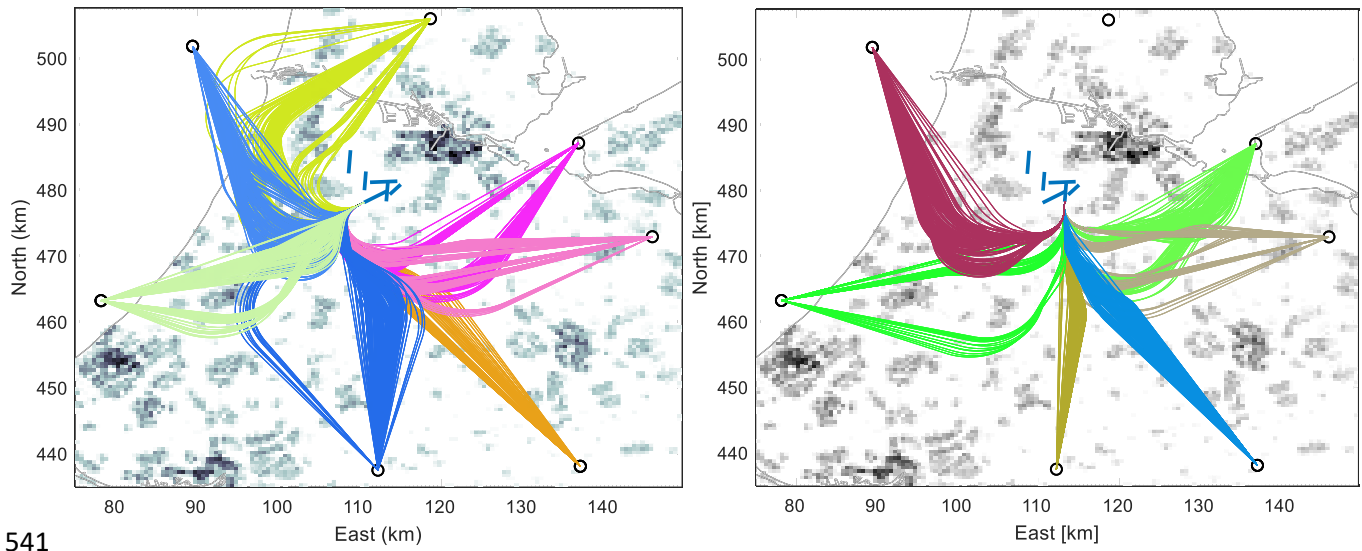


527
528

Fig. 12. Comparison of vertical profiles obtained by the representative solutions.

529
530
531
532
533
534
535
536
537
538
539
540

From noise and fuel perspectives, the optimized routes obtained by the 3D optimization approach are the best candidates and should be used in the set of alternative route options for the distribution problem in the second step. From a practical point of view, however, the implementation of the optimized vertical profiles may prove significantly more difficult. In contrast, NADP1 and NADP2 are the current standard procedures that are widely used. Also, compared with NADP1, NADP2 is generally a better option; however, the difference is small. The differences between their vertical profiles, however, may prove useful in dealing with separation conflicts between aircraft. Therefore, to obtain a better understanding from both a theoretical and a practical perspective, two different scenarios in input data are defined for the optimization problem in the second step. In the first scenario, only the routes obtained by NADP1 and NADP2 are applied, while in the second scenario the routes obtained by all the three types of vertical profiles are used. An overview of ground tracks obtained for all the SIDs originating from RW24 and RW18L in both 2D and 3D optimization scenarios is given in Fig. 13.



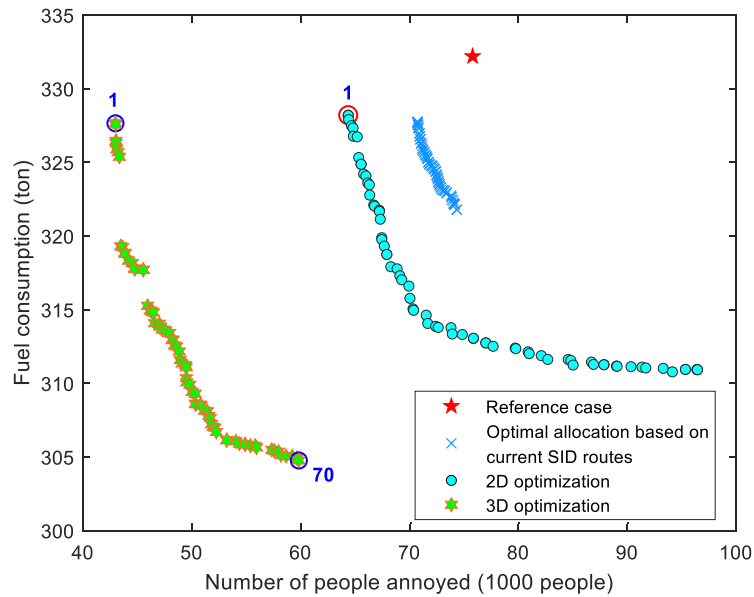
a) RW24
b) RW18L
Fig. 13. Illustration of optimized routes for each SID obtained after Step 1.

544 **5.2.2. Optimized solutions derived from the entire problem**

545 As mentioned earlier, two different sets of input data are considered for the distribution problems in the
 546 second step. Therefore, two distinct optimization problems need to be solved in this section. These
 547 problems are again referred to as 2D and 3D optimization scenarios, respectively. To solve these
 548 problems, the NSGA-II algorithm with a population size of 70 and a maximum number of generations
 549 of 1500, as used in [Ho-Huu et al. \(2019a\)](#), is applied.

550 A closer look at the results obtained for both scenarios reveals that all the solutions obtained by the
 551 3D optimization scenario have a unique route for each SID, while for the solutions obtained by the 2D
 552 optimization scenario, some SIDs require two routes to avoid potential conflicts. In addition, there is no
 553 delay at the runways for all solutions obtained by both approaches. [Fig. 14](#) shows the Pareto-optimized
 554 solutions obtained for the 2D and 3D optimization problems and compares them with the reference case
 555 solution, presented previously in [Section 5.1](#). As expected, the 3D optimization approach provides the
 556 best solutions (denoted as 3D solutions), that significantly outperform the solutions obtained by the 2D
 557 optimization approach (denoted as 2D solutions), as well as those obtained for the reference case, in
 558 terms of both the NPA and fuel consumption.

559



560
561 **Fig. 14.** Comparison of the optimized solutions obtained by the reference case, 2D and 3D optimization.

562 To further analyze the optimized results, three representative solutions, including solution 1 of the
 563 2D optimization scenario and solutions 1 and 70 of the 3D optimization scenario, as highlighted in **Fig.**
 564 **14**, are selected. **Table 5** provides a comparison of specific criteria extracted for these solutions. From
 565 **Table 5**, it can be seen that all the compared metrics obtained by solution 1 (2D optimization) and
 566 solution 70 are better than those found for the reference case. Specifically, solution 1 offers, respectively,
 567 15.08%, 1.20%, 0.96%, and 0.75% reduction in the NPA, fuel consumption, flight distance and flight
 568 time, while the corresponding reductions obtained for solution 70 are, respectively, 21.06%, 8.26%,
 569 8.22% and 8.98%. In a comparison of solution 1 (3D optimization) with the reference case, solution 1
 570 results in a significant decrease in the NPA of about 43.29%, while still saving 1.3% on fuel. Although
 571 there is an increase in the flight distance and elapsed time as a result of longer routes to avoid populated
 572 regions, the use of optimized vertical profiles results in a fuel burn that is still less than that of the
 573 reference case. Note that the purpose of selecting these representative solutions is to merely give insight
 574 into the solution behavior; it does not necessarily imply that the selected solutions should be
 575 recommended to authorities or policymakers. Essentially, the trade-off between criteria and the
 576 subsequent selection of the most desirable solution from the Pareto front is left to the authorities or
 577 policymakers.

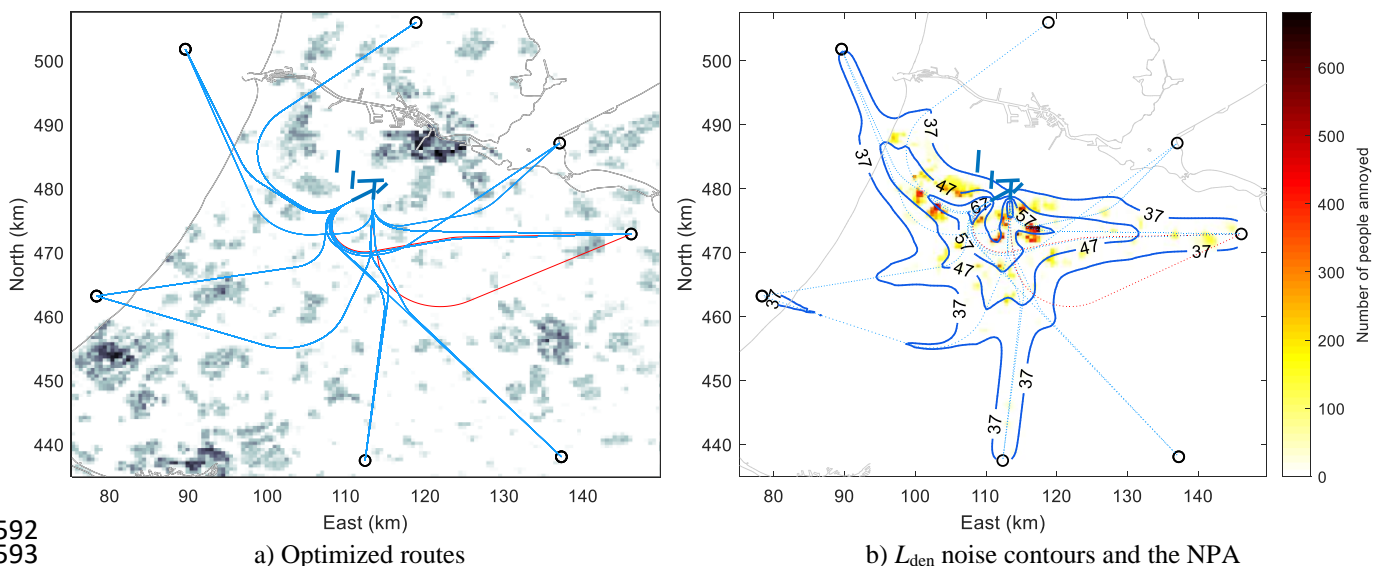
578

579

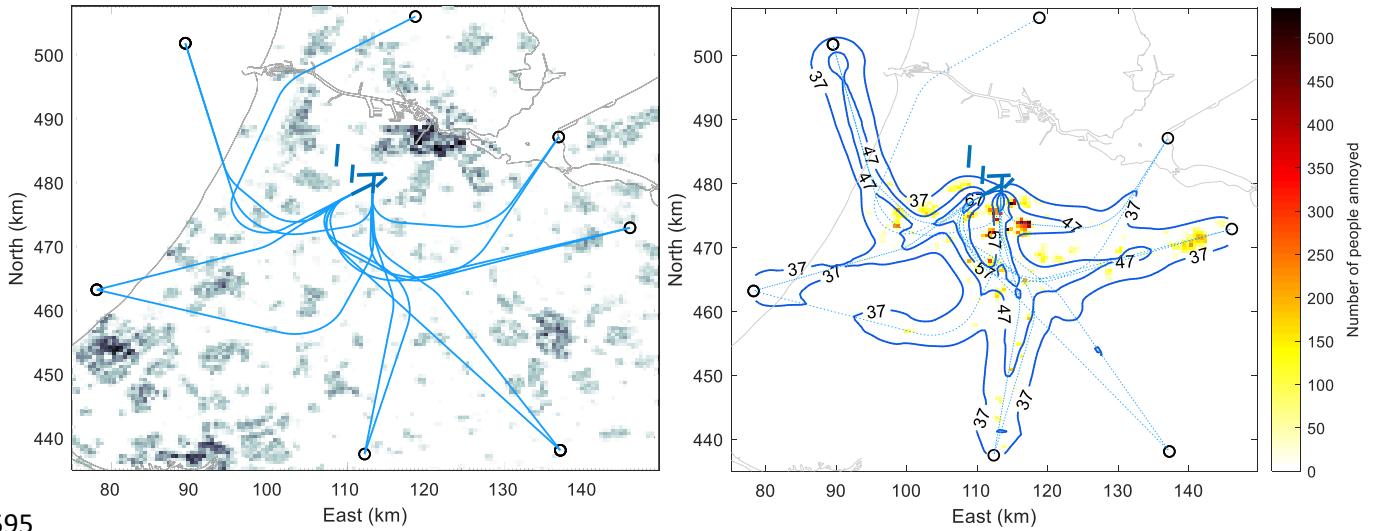
Table 5. Comparison of the criteria of the representative solutions and the reference case.

Criteria	Solution 1 (2D optimization)	Solution 1 (3D optimization)	Solution 70 (3D optimization)	Reference case
Number of people annoyed	64,367	42,985	59,834	75,800
Fuel consumption (ton)	328.21	327.66	304.77	332.20
Flight distance (km)	25,240.57	27,357.49	23,388.53	25,484.13
Flight time (h)	56.71	59.80	52.01	57.14

580 The explanations provided for the comparisons in [Table 5](#) are confirmed by the results shown in
 581 [Figs. 15- 17](#). where the optimized routes, the L_{den} noise contours, and the NPA obtained by the three
 582 solutions are illustrated. A closer look at the optimized routes shows that although the optimized routes
 583 selected by these solutions are different, all of them seek to avoid high-density residential areas and tend
 584 to be close to each other. This results in narrower L_{den} contours and hence a reduced number of people
 585 affected by noise. Another observation is that the routes selected in solutions 1 (both 2D and 3D
 586 optimization) are longer than those selected by solution 70. This is according to expectations, as both
 587 solutions for 1 are noise-preferred solutions, and hence their routes tend to be longer to avoid populated
 588 regions. In contrast, solution 70 is a fuel-preferred solution and therefore prefers to choose shorter routes
 589 to reduce the fuel burn. Note that the red routes in [Fig. 15](#) (solution 1 of 2D problem) are two alternative
 590 routes that are only used by some conflicting flights, whilst the remainder of the scheduled flights make
 591 use of one of the blue routes for each SID.



594 **Fig. 15.** Illustration of the optimized routes, the L_{den} noise contours, and the NPA (solution 1 – 2D optimization).

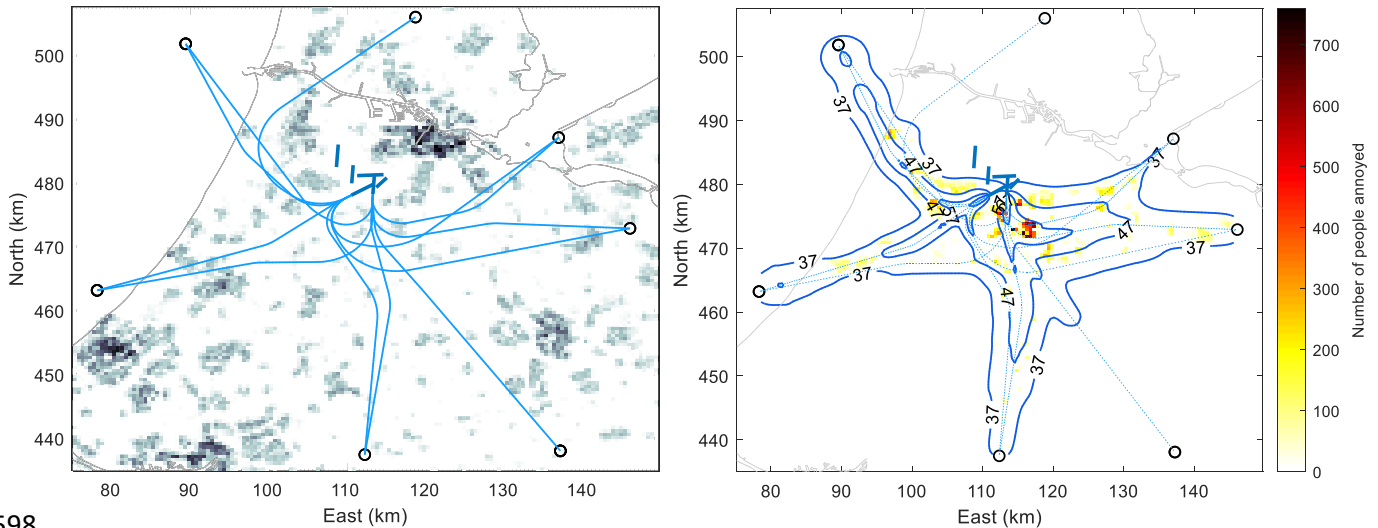


595
596
597

a) Optimized routes

b) L_{den} noise contours and the NPA

Fig. 16. Illustration of the optimized routes, the L_{den} noise contours, and the NPA (solution 1 – 3D optimization).



598
599
600

a) Optimized routes

b) L_{den} noise contours and the NPA

Fig. 17. Illustration of the optimized routes, the L_{den} noise contours, and the NPA (solution 70 – 3D optimization).

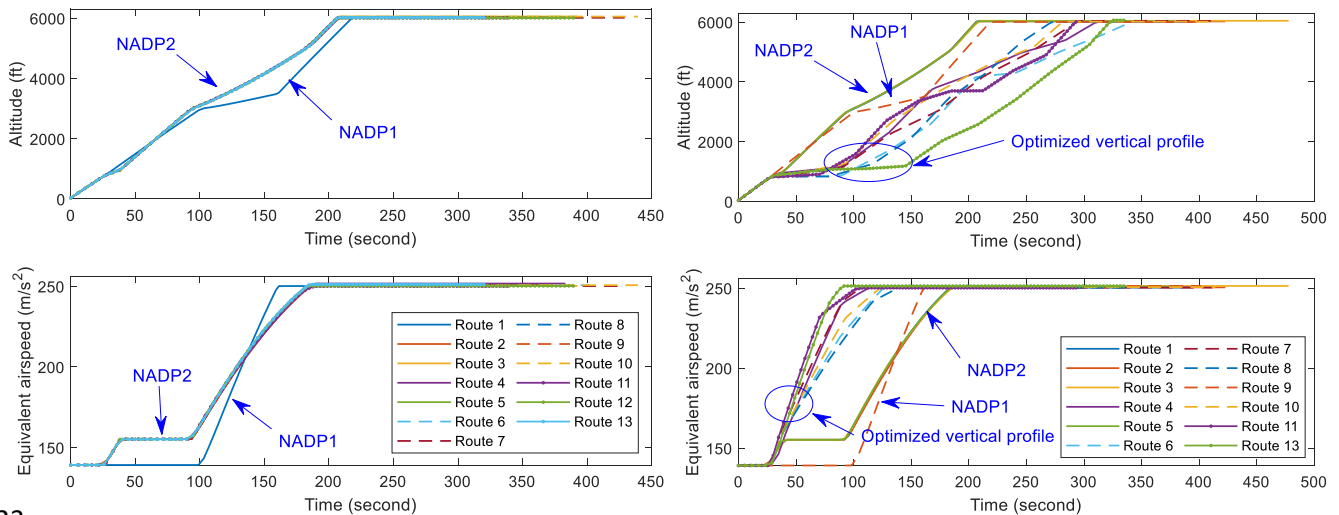
601 **Table 6** provides the detailed distribution of flights among the optimized routes obtained in the
 602 selected solutions. It should be noted that as the selection of routes and the distribution of flights among
 603 these routes are optimized simultaneously, each solution will have its own optimized combination of
 604 selected routes and flight distribution. Therefore, it is difficult to make a direct comparison regarding
 605 the aircraft distribution between them, especially the comparison between 2D and 3D solutions. As a
 606 result, **Table 6** merely aims to give insight into the optimized solution behavior, rather than serving as a
 607 basis for comparison.

Table 6. Distribution of flights to the optimized routes obtained by the 2D and 3D representative solutions.

Route number	Solution	Day			Evening			Night		
		F100	B738	B773	F100	B738	B773	F100	B738	B773
1	1 (2D)	6	0	0	0	0	0	0	0	0
	1 (3D)	4	11	0	0	4	1	0	2	0
	70 (3D)	12	11	2	1	4	3	5	2	0
2	1 (2D)	3	1	0	0	0	0	7	2	0
	1 (3D)	0	0	3	0	0	4	6	0	0
	70 (3D)	0	0	1	0	0	2	2	0	0
3	1 (2D)	23	13	3	6	6	5	0	0	0
	1 (3D)	28	3	0	6	2	0	1	0	0
	70 (3D)	20	3	0	5	2	0	0	0	0
4	1 (2D)	5	38	9	1	5	8	0	19	3
	1 (3D)	30	37	15	4	4	10	8	19	2
	70 (3D)	4	11	4	0	1	6	0	1	0
5	1 (2D)	52	31	19	8	5	4	8	0	0
	1 (3D)	27	32	13	5	6	2	0	0	1
	70 (3D)	53	58	24	9	9	6	8	18	3
6	1 (2D)	2	7	2	2	1	0	0	1	0
	1 (3D)	2	9	1	2	1	0	0	1	0
	70 (3D)	4	9	2	2	1	0	1	1	0
7	1 (2D)	2	2	0	0	0	0	1	0	0
	1 (3D)	2	0	1	0	0	0	1	0	0
	70 (3D)	0	0	0	0	0	0	0	0	0
8	1 (2D)	25	16	3	2	5	0	2	0	0
	1 (3D)	28	44	3	2	7	0	2	22	0
	70 (3D)	28	44	3	2	7	0	2	22	0
9	1 (2D)	5	30	0	1	3	0	0	22	0
	1 (3D)	2	2	0	1	1	0	0	0	0
	70 (3D)	2	2	0	1	1	0	0	0	0
10	1 (2D)	12	19	4	0	2	1	5	3	1
	1 (3D)	9	17	1	0	2	1	5	3	1
	70 (3D)	3	9	0	0	0	0	1	1	0
11	1 (2D)	15	5	6	4	2	0	0	0	0
	1 (3D)	18	7	9	4	2	0	0	0	0
	70 (3D)	24	15	10	4	4	1	4	2	1
12	1 (2D)	0	7	0	0	2	0	1	1	0
	1 (3D)	0	2	0	0	1	0	0	0	0
	70 (3D)	0	3	0	0	0	0	0	0	0
13	1 (2D)	27	11	35	4	5	0	2	0	1
	1 (3D)	27	16	35	4	6	0	3	1	1
	70 (3D)	27	15	35	4	7	0	3	1	1

609 In order to make the comparison regarding the vertical profiles more transparent, the representative
610 vertical profiles of a Fokker 100 obtained for solutions 1 (both 2D and 3D optimization) are depicted in
611 [Fig. 18](#). As expected, despite not having the best performance in terms of either noise or fuel burn,
612 NADP1 is still selected in both the 2D and 3D solutions, merely because it helps avoid conflicts.
613 However, due to its poor performance, it is rarely used. More specifically, for both the 2D and 3D
614 solutions, only 1 route selects NADP1 as the optimized option, while the remainder chooses either
615 NADP2 or the optimized vertical profiles. The selection of NADP1 has shown that the separation
616 requirement is an important and challenging issue that will be very difficult to solve if only one type of
617 vertical profiles is available for all aircraft movements, especially for operations at peak hours. This

618 issue again can be seen in the 3D solution. In this solution, even though the optimized vertical profile
 619 offers the best performance in both criteria, only 7 routes use it as the optimized option, while there are
 620 still 4 routes using NADP2 and 1 route using NADP1. Thanks to the combination of all three different
 621 vertical profiles, the 3D optimized solutions are the only ones that offer conflict-free solutions by using
 622 only one route for each SID for the entire flight schedule.



623 a) Solution 1 (2D optimization) b) Solution 1 (3D optimization)
 624 Fig. 18. Comparison of the vertical profiles of Fokker 100 obtained by 2D and 3D optimization.
 625
 626

627 **6. Conclusions**

628 In this paper, we have presented a multilevel optimization framework for the design of optimal departure
 629 routes and the distribution of aircraft movements among these routes, while taking the sequence and
 630 separation constraints of aircraft into account. The proposed framework consists of two successive steps:
 631 1) the design of optimal routes for each SID, and 2) the selection and distribution of flights among these
 632 routes. In order to deal with the sequence and separation requirements for aircraft, a runway assignment
 633 model, a conflict detection algorithm, and a rerouting technique have also been developed.

634 The performance and applicability of the proposed framework have been demonstrated through a
 635 case study at Amsterdam Airport Schiphol (AMS) in The Netherlands. In this case study, the departure
 636 operations for an entire day, featuring 599 flights and 13 distinct routes, have been considered. First, to
 637 validate the integration of the runway assignment model and the conflict detection algorithm into the
 638 allocation model in Step 2, a pure allocation problem based on the current SIDs has been executed. The

639 obtained results reveal that the distribution model is reliable and able to provide better options that help
640 significantly reduce the noise impact and fuel consumption compared with the reference case.
641 Subsequently, optimized solutions have been generated using the fully integrated framework. In order
642 to provide a better view from both theoretical and practical perspectives, two different settings of input
643 data for the distribution model in Step 2 have also been assessed. The numerical results have revealed
644 that both problems can provide solutions that are much better in terms of both noise and fuel, relative to
645 the reference case. Also, the 3D optimization approach significantly outperforms the 2D optimization
646 approach.

647 In view of the attained favorable results, the framework appears to be suitable for expansion to other
648 applications such as the design of arrival routes and the allocation of flights among these routes, and the
649 problem that considers both departure and arrival operations concurrently. Moreover, instead of using
650 the rerouting technique in the developed framework, at some occasions, Air Traffic Controllers could
651 implement small delays on the ground or slow down or speed up one of the conflicting flights without
652 changing the given SIDs to avoid conflict in the air. These considerations can also be integrated into the
653 developed framework in future research. In addition, since the results obtained by the framework are
654 Pareto solutions, it is a challenge for potential users to choose a suitable solution from a given Pareto
655 front. Therefore, the development of selection methods and more in-depth analyses of the optimized
656 results are necessary in future work.

657 **References**

- 658 Asensio, C., Gasco, L., de Arcas, G., 2017. A Review of Non-Acoustic Measures to Handle Community
659 Response to Noise around Airports. *Curr. Pollut. Reports* 230–244. [https://doi.org/10.1007/s40726-017-](https://doi.org/10.1007/s40726-017-0060-x)
660 [0060-x](https://doi.org/10.1007/s40726-017-0060-x)
- 661 Boeing, 2016. Current Market Outlook 2016–2035.
- 662 Braakenburg, M.L., Hartjes, S., Visser, H.G., 2011. Development of a Multi-Event Trajectory Optimization Tool
663 for Noise-Optimized Approach Route Design. *AIAA J.* 1–13. <https://doi.org/10.2514/6.2011-6929>
- 664 Casalino, D., Diozzi, F., Sannino, R., Paonessa, A., 2008. Aircraft noise reduction technologies: A bibliographic
665 review. *Aerosp. Sci. Technol.* 12, 1–17. <https://doi.org/10.1016/j.ast.2007.10.004>
- 666 Centraal Bureau voor de Statistiek. Dataset bevolkingsdichtheid. [https://www.cbs.nl/nl-nl/dossier/nederland-](https://www.cbs.nl/nl-nl/dossier/nederland-regionaal/geografische-data)
667 [regionaal/geografische-data](https://www.cbs.nl/nl-nl/dossier/nederland-regionaal/geografische-data). Online, accessed 2016-10-20.
- 668 Chatelain, P., Van Vyve, M., 2018. Modeling fair air traffic assignment in the vicinity of airports. *Transp. Res.*
669 *Part D Transp. Environ.* 65, 213–228. <https://doi.org/10.1016/j.trd.2018.08.016>
- 670 D’Ariano, A., Pacciarelli, D., Pistelli, M., Pranzo, M., 2015. Real-time scheduling of aircraft arrivals and
671 departures in a terminal maneuvering area. *Networks*, 65(3) 212–227. <https://doi.org/10.1002/net.21599>
- 672 Deb, K., Pratap, A., Agarwal, S., Meyarivan, T., 2002. A fast and elitist multiobjective genetic algorithm:
673 NSGA-II. *IEEE Trans. Evol. Comput.* 6, 182–197. <https://doi.org/10.1109/4235.996017>
- 674 J.G. Delsen., 2016. Flexible Arrival & Departure Runway Allocation Using Mixed-Integer Linear Programming:

675 A Schiphol Airport Case Study, MSc. thesis, Delft University of Technology.

676 Dons, J., 2012. Optimization of Departure and Arrival Routing for Amsterdam Airport Schiphol- A Noise
677 Abatement Study. MSc. thesis, Delft University of Technology.

678 ECAC, 2016. ECAC/CEAC Doc 29 4th Edition Report on Standard Method of Computing Noise Contours
679 around Civil Airports Volume 1: Applications Guide 1.

680 EUROCONTROL, 2014b. User Manual for the Base of Aircraft Data (BADA) Rev. 3.12, EEC
681 Technical/Scientific Report No. 12/11/22-58.

682 EUROCONTROL, 2018. RECAT-EU - European Wake Turbulence Categorisation and Separation Minima on
683 Approach and Departure. Brussels. [http://www.recat-project.eu/sites/default/files/20180214_recat-
684 eu_presentation_brochure_v1.2.pdf](http://www.recat-project.eu/sites/default/files/20180214_recat-eu_presentation_brochure_v1.2.pdf)

685 European Environment Agency (EEA), 2010. Good practice guide on noise exposure and potential health effects,
686 n.d. , in: EEA Technical Report.

687 Filippone, A., 2014. Aircraft noise prediction. *Prog. Aerosp. Sci.* 68, 27–63.
688 <https://doi.org/10.1016/j.paerosci.2014.02.001>

689 Frair, L., 1984. Airport noise modelling and aircraft scheduling so as to minimize community annoyance. *Appl.*
690 *Math. Model.* 8, 271–281. [https://doi.org/10.1016/0307-904X\(84\)90162-8](https://doi.org/10.1016/0307-904X(84)90162-8)

691 Ganić, E., Babić, O., Čangalović, M., Stanojević, M., 2018. Air traffic assignment to reduce population noise
692 exposure using activity-based approach. *Transp. Res. Part D Transp. Environ.* 63, 58–71.
693 <https://doi.org/10.1016/j.trd.2018.04.012>

694 Gardi, A., Sabatini, R., Ramasamy, S., 2015. Multi-objective optimisation of aircraft flight trajectories in the
695 ATM and avionics context. *Prog. Aerosp. Sci.* 83, 1–36. <https://doi.org/10.1016/j.paerosci.2015.11.006>

696 Hartjes, S., Dons, J., Visser, H.G., 2014. Optimization of Area Navigation Arrival Routes for Cumulative Noise
697 Exposure. *J. Aircr.* 51, 1432–1438. <https://doi.org/10.2514/1.C032302>

698 Hartjes, S., Visser, H., 2016. Efficient trajectory parameterization for environmental optimization of departure
699 flight paths using a genetic algorithm. *Proc. Inst. Mech. Eng. Part G J. Aerosp. Eng.* 0, 1–9.
700 <https://doi.org/10.1177/0954410016648980>

701 Hartjes, S., Visser, H.G., Hebly, S.J., 2010. Optimisation of RNAV noise and emission abatement standard
702 instrument departures. *Aeronaut. J.* 114, 757–767. <https://doi.org/10.1017/CBO9781107415324.004>

703 Ho-Huu, V., Ganić, E., Hartjes, S., Babić, O., Curran, R., 2019a. Air traff assignment based on daily population
704 mobility to reduce aircraft noise effects and fuel consumption. *Transp. Res. Part D Transp. Environ.* 72,
705 127–147. <https://doi.org/10.1016/j.trd.2019.04.007>

706 Ho-Huu, V., Hartjes, S., Visser, H., Curran, R., 2017. An Efficient Application of the MOEA/D Algorithm for
707 Designing Noise Abatement Departure Trajectories. *Aerospace* 4, 54.
708 <https://doi.org/10.3390/aerospace4040054>

709 Ho-Huu, V., Hartjes, S., Visser, H.G., Curran, R., 2019b. An optimization framework for the design and
710 allocation of aircraft to multiple departure routes. *Transp. Res. Part D Transp. Environ.* 76, 273-288.
711 <https://doi.org/10.1016/j.trd.2019.10.003>

712 Ho-Huu, V., Hartjes, S., Visser, H.G., Curran, R., 2018. Integrated design and allocation of optimal aircraft
713 departure routes. *Transp. Res. Part D Transp. Environ.* 63, 689–705.
714 <https://doi.org/10.1016/j.trd.2018.07.006>

715 Hogenhuis, R.H., Hebly, S.J., Visser, H.G., 2011. Optimization of area navigation noise abatement approach
716 trajectories. *Proc. Inst. Mech. Eng. Part G-Journal Aerosp. Eng.* 225, 513–521.
717 <https://doi.org/10.1177/09544100JAERO840>

718 International Civil Aviation Organization (ICAO), 2006a. Procedures for air navigation services – Aircraft
719 operations. Vol. I, Flight Procedures.

720 International Civil Aviation Organization (ICAO), 2016b. Doc 4444 – Procedures for air navigation services –
721 Air traffic management. Sixteenth Edition. Montreal, QC, Canada.

722 Isaacson, D.R., Erzberger, H., 1997. Design of a conflict detection algorithm for the Center/TRACON
723 automation system, in: 16th DASC. AIAA/IEEE Digital Avionics Systems Conference. Reflections to the
724 Future. Proceedings. pp. 9.3–1. <https://doi.org/10.1109/DASC.1997.637306>

725 Janssen, S.A., Centen, M.R., Vos, H., Van Kamp, I., 2014. The effect of the number of aircraft noise events on
726 sleep quality. *Appl. Acoust.* 84, 9–16. <https://doi.org/10.1016/j.apacoust.2014.04.002>

727 Kuiper, B.R., Visser, H.G., Heblj, S., 2012. Efficient use of an allotted airport annual noise budget through
728 minimax optimization of runway allocations. *Proc. Inst. Mech. Eng. Part G J. Aerosp. Eng.* 227, 1021–
729 1035. <https://doi.org/10.1177/0954410012447767>

730 Morrell, S., Taylor, R., Lyle, D., 1997. A review of health effects of aircraft noise. *Aust. N. Z. J. Public Health*
731 21, 221–236. <https://doi.org/10.1111/j.1467-842X.1997.tb01690.x>

732 Prats, X., Puig, V., Quevedo, J., 2011. Equitable Aircraft Noise-Abatement Departure Procedures. *J. Guid.*
733 *Control. Dyn.* 34, 192–203. <https://doi.org/10.2514/1.49530>

734 Prats, X., Puig, V., Quevedo, J., Nejari, F., 2010a. Lexicographic optimisation for optimal departure aircraft

735 trajectories. *Aerosp. Sci. Technol.* 14, 26–37. <https://doi.org/10.1016/j.ast.2009.11.003>

736 Prats, X., Puig, V., Quevedo, J., Nejjari, F., 2010b. Multi-objective optimisation for aircraft departure trajectories

737 minimising noise annoyance. *Transp. Res. Part C Emerg. Technol.* 18, 975–989.

738 <https://doi.org/10.1016/j.trc.2010.03.001>

739 Rodríguez-Díaz, A., Adenso-Díaz, B., González-Torre, P.L., 2017. A review of the impact of noise restrictions at

740 airports. *Transp. Res. Part D Transp. Environ.* 50, 144–153. <https://doi.org/10.1016/j.trd.2016.10.025>

741 Samà, M., D’Ariano, A., D’Ariano, P., Pacciarelli, D., 2017a. Scheduling models for optimal aircraft traffic

742 control at busy airports: tardiness, priorities, equity and violations considerations. *Omega* 67(1), 81–98.

743 <https://doi.org/10.1016/j.omega.2016.04.003>

744 Samà, M., D’Ariano, A., Corman, F., Pacciarelli, D., 2017b. Metaheuristics for efficient aircraft scheduling and

745 re-routing at busy terminal control areas. *Transp. Res. Part C* 80 (1), 485–511.

746 <https://doi.org/10.1016/j.trc.2016.08.012>

747 Samà, M., D’Ariano, A., Corman, F., Pacciarelli, D., 2018. Coordination of scheduling decisions in the

748 management of airport airspace and taxiway operations, *Transp. Res. Proce.* 23, 246-262.

749 <https://doi.org/10.1016/j.trpro.2017.05.015>

750 Samà, M., D’Ariano, A., Palagachev, K., Gerdtts, M., 2019. Integration methods for aircraft scheduling and

751 trajectory optimization at a busy terminal manoeuvring area. *OR Spec.* 41, 641–681.

752 <https://doi.org/10.1007/s00291-019-00560-1>

753 Song, Z., Visser, H.G., Mingshan, H., Wei, C., 2014. Optimized Multi-Event Simultaneous Departure Routes for

754 Major Hub Airport. *Int. J. Model. Optim.* 4, 482–488. <https://doi.org/10.7763/IJMO.2014.V4.421>

755 Storn, R., Price, K., 1997. Differential Evolution – A Simple and Efficient Heuristic for global Optimization over

756 Continuous Spaces. *J. Glob. Optim.* 11, 341–359. <https://doi.org/10.1023/A:1008202821328>

757 Torres, R., Chaptal, J., Bès, C., Hiriart-Urruty, J.-B., 2011. Optimal , Environmentally Friendly Departure

758 Procedures for Civil Aircraft. *J. Aircr.* 48, 11–23. <https://doi.org/10.2514/1.C031012>

759 Visser, H.G., 2008. Environmentally optimized resolutions of in-trail separation conflicts for arrival flights. *J.*

760 *Aircr.* 45, 1198–1205. <https://doi.org/10.2514/1.34090>

761 Visser, H.G., Wijnen, R.A.A., 2003. Optimisation of noise abatement arrival trajectories. *Aeronaut. J.* 107, 607–

762 615. <https://doi.org/10.1017/S0001924000013828>

763 Visser, H.G., Wijnen, R.A.A., 2001. Optimization of Noise Abatement Departure Trajectories. *J. Aircr.* 38, 620–

764 627. <https://doi.org/10.2514/2.2838>

765 Yu, H., Van Kampen, E.-J., Mulder, J.A., 2016. An Optimization Paradigm for Arrival Trajectories

766 using Trajectory Segmentation and State Parameterization. *AIAA Guid. Navig. Control Conf.* 1–17.

767 <https://doi.org/10.2514/6.2016-1872>

768 Zachary, D.S., Gervais, J., Leopold, U., 2010. Multi-impact optimization to reduce aviation noise and emissions.

769 *Transp. Res. Part D Transp. Environ.* 15, 82–93. <https://doi.org/10.1016/j.trd.2009.09.005>

770 Zachary, D.S., Gervais, J., Leopold, U., Schutz, G., Huck, V.S.T., Braun, C., 2011. Strategic Planning of Aircraft

771 Movements with a Three-Cost Objective. *J. Aircr.* 48, 256–264. <https://doi.org/10.2514/1.C031090>

772 Zaporozhets, O.I., Tokarev, V.I., 1998. Predicted flight procedures for minimum noise impact. *Appl. Acoust.* 55,

773 129–143. [http://dx.doi.org/10.1016/S0003-682X\(97\)00108-4](http://dx.doi.org/10.1016/S0003-682X(97)00108-4)

774 Zhang, M., Filippone, A., Bojdo, N., 2018. Multi-objective optimisation of aircraft departure trajectories.

775 *Aerosp. Sci. Technol.* 79, 37–47. <https://doi.org/10.1016/j.ast.2018.05.032>

776 Zhang, Q., Li, H., 2007. MOEA/D: A Multiobjective Evolutionary Algorithm Based on Decomposition. *IEEE*

777 *Trans. Evol. Comput.* 11, 712–731. <https://doi.org/10.1109/TEVC.2007.892759>